

Efficient mid-term forecasting of hourly electricity load using generalized additive models

Monika Zimmermann^{a,*}, Florian Ziel^a

*^aChair of Environmental Economics, esp. Economics of Renewable Energy
University of Duisburg-Essen
Germany*

Abstract

Accurate mid-term (weeks to one year) hourly electricity load forecasts are essential for strategic decision-making in power plant operation, ensuring supply security and grid stability, and energy trading. While numerous models effectively predict short-term (hours to a few days) hourly load, mid-term forecasting solutions remain scarce. In mid-term load forecasting, besides daily, weekly, and annual seasonal and autoregressive effects, capturing weather and holiday effects, as well as socio-economic non-stationarities in the data, poses significant modeling challenges. To address these challenges, we propose a novel forecasting method using Generalized Additive Models (GAMs) built from interpretable P-splines and enhanced with autoregressive post-processing. This model uses smoothed temperatures, Error-Trend-Seasonal (ETS) modeled non-stationary states, a nuanced representation of holiday effects with weekday variations, and seasonal information as input. The proposed model is evaluated on load data from 24 European countries. This analysis demonstrates that the model not only has significantly enhanced forecasting accuracy compared to state-of-the-art methods but also offers valuable insights into the influence of individual components on predicted load, given its full interpretability. Achieving performance akin to day-ahead TSO forecasts in fast computation times of a few seconds for several years of hourly data underscores the model's potential for practical application in the power system industry.

Keywords: Electricity Demand, GAM, Error-Trend-Seasonal Model, Weather, Holidays, Trend Behavior

1. Introduction

Accurate mid-term electricity load forecasts (weeks to one year), specifically, of an hourly resolution are crucial for all stakeholders in the power sector. They guide electricity utilities in production and maintenance planning, ensuring grid stability and uninterrupted supply. They are essential for energy trading and investment firms to make informed decisions. They are instrumental in facilitating policymakers to a sensitive and socially acceptable transition from fossil fuels to electric power sources, particularly in sectors like transportation and heating.

For these tasks the need for, specifically, hourly resolution forecasts arises from the dynamics of the electricity market. Electricity markets commonly operate at hourly or even finer resolution accounting for

*Corresponding author

Email addresses: Monika.Zimmermann@uni-due.de (Monika Zimmermann), Florian.Ziel@uni-due.de (Florian Ziel)

the inter-day fluctuations in electricity demand and supply. On the demand side, these are attributed to our western society's hour-specific daily living and working behavior. On the supply side, they are caused by an increased share of renewables in the market. Consequently, coarser-resolution forecasts would fail to meet the required accuracy level for stakeholders to effectively fulfill their tasks in the power sector, as argued by [Behm et al. \(2020\)](#); [Agrawal et al. \(2018\)](#).

While extensive research exists on hourly short-term (hours to a few days) load forecasting, the overview by [Verwiebe et al. \(2021\)](#) or [Davis et al. \(2016\)](#) suggests that literature remains scarce for hourly mid-term forecasts. This gap can be attributed to the central role of weather, in particular air temperature, in driving electricity demand contrasted by the lack of exact weather forecasts for a medium horizon, see e.g. [Bashiri Behmiri et al. \(2023\)](#); [Kalhori et al. \(2022\)](#); [Agrawal et al. \(2018\)](#); [De Felice et al. \(2015\)](#); [Ghiassi et al. \(2006\)](#), and the multifaceted nature of load time series. Following a classification proposed by [Pierrot & Goude \(2011\)](#), the various facets underlying load can be consolidated into three main groups:

- (i) **Calender Characteristics:** These encompass the calender-based behavior of modern western societies entailing repetitive patterns of different seasonalities in electricity load, e.g. yearly patterns (decreased load during public and banking holidays, vacation periods), weekly patterns (higher load levels on weekdays vs. lower load levels on weekends), and daily patterns (higher load during the day vs. lower load during the night, load peaks during lunch- and dinnertime).
- (ii) **Weather Characteristics:** These include air temperature, humidity, cloud cover, wind speed, and day length that affect load due to their impact on electric heating and lighting.
- (iii) **Socio-Economic Characteristics:** These involve macroeconomic, socioeconomic and energy variables, e.g. economic growth, industrial production, population size or fossil fuel prices, which influence, in particular in their unit root behavior, medium to long-term levels of load.

Proposed methods in mid-term load forecasting range from classical time series, see e.g. [Petropoulos et al. \(2022\)](#) for a concise overview, to sophisticated machine learning models based on e.g. different types of neural networks, gradient boosting machines or random forests, see e.g. the highly cited winning method of a EUNITE Competition [Chen et al. \(2004\)](#) or [Bashiri Behmiri et al. \(2023\)](#); [Zhang et al. \(2023\)](#); [Li et al. \(2023\)](#); [Kalhori et al. \(2022\)](#); [Butt et al. \(2022\)](#); [Oreshkin et al. \(2021\)](#); [Han et al. \(2019\)](#); [Agrawal et al. \(2018\)](#); [Bouktif et al. \(2018\)](#). Furthermore, hybrid models combining diverse forecasting methods have emerged lately, as summarized by [Petropoulos et al. \(2022\)](#) and [Hong et al. \(2016\)](#). For instance, winning methods in the IEEE DataPort Competition, see [De Vilmarest & Goude \(2022\)](#); [Ziel \(2022\)](#), employed combinations of different techniques, including Generalized Additive Models (GAMs). Notably, in [De Vilmarest & Goude \(2022\)](#), GAMs exhibited the lowest forecasting errors compared to other ensembled forecasting models, e.g. autoregressive, linear regression, and Multi-Layer Perceptron models.

Similarly, GAMs have consistently demonstrated outstanding performance in previous forecasting competitions, such as achieving top-three results, see [Nedellec et al. \(2014\)](#), in GEFCom 2012 [Davis et al. \(2014\)](#), and securing the top two spots, see [Gaillard et al. \(2016\)](#); [Dordonnat et al. \(2016\)](#), in GEFCom

2014 [Hong et al. \(2016\)](#). Motivated by the success of GAMs in load forecasting competitions alongside the effectiveness of early GAM-based methods in load forecasting, see e.g. [Pierrot & Goude \(2011\)](#); [Fan & Hyndman \(2012\)](#); [Goude et al. \(2014\)](#), we adopt this framework as the foundation for our proposed load forecasting model.

Generalized Additive Models offer a distinctive blend of interpretability and efficient estimation while capturing non-linear relationships. This stems from their underlying linearity, i.e. a linear model structure, in non-linear functions. This combination of attributes makes them a compelling choice when computational efficiency and model understanding are crucial and consequently suitable as weak learners, e.g. as input for neural networks, and as input in ensembling methods, see [Lepore et al. \(2022\)](#).

Specifically, we propose a two-stage GAM built from interpretable P-splines that is enhanced with autoregressive post-processing. This model uses exponentially smoothed temperatures, Error-Trend-Seasonal (ETS) modeled non-stationary states, a nuanced representation of holiday effects with weekday variations, and seasonal information as inputs. With this approach, we contribute five key innovations to the field of mid-term hourly load forecasting:

- (i) **Accurate, Fast and Interpretable Model:** We develop a GAM-based forecasting model utilizing shrinkage and discretization that covers all relevant characteristics of load while maintaining computation times of a few seconds for hourly year-ahead forecasts. The model is interpretable in each input characteristic, allowing us to derive the effect of holidays and weather inputs. It has superior forecasting accuracy compared to state-of-the-art methods.
- (ii) **Individual Holiday Modeling:** We introduce a novel modeling approach that captures the effect induced by each holiday individually through a holiday-specific activation variable. This approach enables the modeling of holidays limited to a specific region of a country as well as holiday periods such as the Christmas/New Year vacation period. Moreover, we distinguish the effects of holidays that occur on a fixed date (e.g. New Year’s Day) from those that occur on a fixed weekday (e.g. Good Friday).
- (iii) **Mid-Term Temperature Effects:** We show that the incorporation of temperature information improves the mid-term forecasting accuracy significantly even though our simple mid-term temperature forecasts provide essentially only seasonal patterns.
- (iv) **Mid-Term State Components:** To account for the mid-term gradual change of load levels due to economic or socioeconomic factors, we incorporate ETS modelled state components in our model that have a persistent trend behavior.
- (v) **Comprehensive Robustness Check:** The model’s robustness is demonstrated through an extensive evaluation across 24 European countries¹, illustrated by the Map 1, over more than 9 years (2015-2024), including volatile periods due to the COVID-19 pandemic and the energy crisis caused by the Russian invasion of Ukraine.

¹While data from all European countries participating in ENTSOE was initially collected, some countries were ultimately excluded from the analysis due to data quality issues.

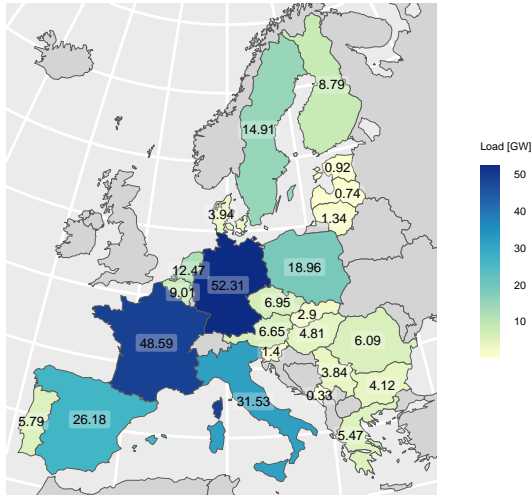


Figure 1: Average load of 2023 in the 24 European countries considered in the study.

In a forecasting study, we found that our proposed model has superior accuracy compared to a set of 8 common benchmark models and compared to the same model excluding temperature and holiday effects. Regarding the inclusion of the ETS state components improvement is diminished in many countries during the first lockdowns due to COVID. For a quarter of the considered countries, accuracy reaches the range of the short-term day-ahead TSO forecasts which highlights the applicability of our model in the electricity utilities industry.

The remainder of this paper is organized as follows: Section 2 details the multifaceted characteristics of load time series. Section 3 describes the Methodology, with a concise theoretical back-

ground on GAM and additive autoregressive models in 3.1 and 3.2, respectively, a conceptual overview of our model in 3.3, data preprocessing in 3.4 and specification, estimation and forecasting of our model in 3.5-3.6. Benchmark models are detailed in Chapter 3.7, and the forecasting study and evaluation design in Chapter 4. The results of the comprehensive forecasting study are discussed and interpreted in Section 5. Finally, Section 6 concludes and outlines further research to be build upon this work.

2. Data

2.1. Electricity Load

The load data used for this study were retrieved from ENTSOE, cover the period from January 1st, 2015 to February 17th, 2024 and are available for all considered countries in an hourly resolution. This data incorporates implicit calendar and time information, including daily, weekly, and annual seasonalities, as well as changes due to daylight saving time and leap years.

The load profiles exhibit strong seasonal patterns across daily, weekly, and annual timescales, as shown by Figures 2 and 3. These patterns include lower loads during summer compared to winter months, higher loads on weekdays compared to weekends, and lower loads at night compared to daytime. Consequently, autocorrelation is high for the most recent lags, lags of the neighboring hours on the previous day and the previous week. Notably, yearly seasonal variations are more pronounced in France due to the country’s reliance on electric heating.

Load is influenced by past observations not only in terms of its autoregressive components but also in terms of its previous mid-term level. More precisely, random shocks (e.g. due to a financial crisis, carbon tax, technological advancements, supply shortages, or large-scale migration caused by war) on load can cause permanent deviations from a predetermined equilibrium level. Since electricity demand is strongly tied to the economy, load inherits the prevalence of these shocks via transmission flows from

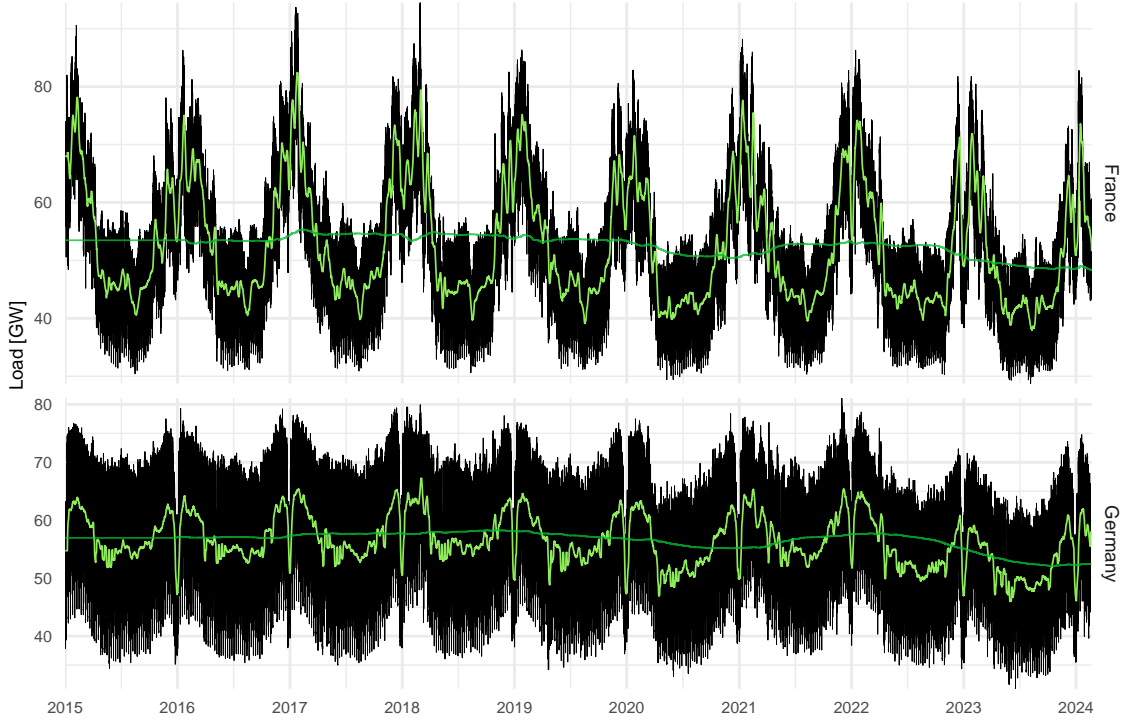


Figure 2: Hourly load (black), weekly (light green) and yearly, i.e. 52 weeks, (dark green) moving average load from January 1st, 2015 to February 17th, 2024.

key macroeconomic, socioeconomic and energy variables [Schneider & Strielkowski \(2023\)](#); [Hendry & Juselius \(2000\)](#); [Smyth \(2013\)](#). Key macroeconomic drivers of electricity demand are, for instance, Gross Domestic Product, employment rate, Consumer Price Index and Industrial Production Index measuring economic well-being, purchasing power, and production output of manufacturing and utilities. These macroeconomic variables, with GDP being a prime example, see [Kalhori et al. \(2022\)](#); [Harvey et al. \(2007\)](#), are generally recognized to exhibit persistent shifts in their level component. This has been, firstly, evidenced by the seminal work of [Nelson & Plosser \(1982\)](#) and mostly supported by revisiting studies, see e.g. [Gil-Alaña & Robinson \(1997\)](#); [Perron \(1997\)](#) among others. Socioeconomic and energy variables affecting load are, for instance, population size and fossil fuel prices. Similar to macroeconomic variables, these factors are predominantly recognized to exhibit a permanent shift in levels, see e.g. [Smyth \(2013\)](#) for a literature overview and [Schneider & Strielkowski \(2023\)](#); [Narayan & Liu \(2015\)](#) on energy variables.

Prevailing shifts in the level component, defined in time series decomposition as the average value over a specific timeframe, see [Svetunkov \(2023\)](#) for details, contribute to the non-stationarity of load data. Recall that non-stationary time series exhibit fluctuations in their statistical properties (mean, variance, and autocorrelation) over time. By differencing the load time series, its level component can be stabilized. This form of non-stationarity is known as a unit root.

Following the illustration of a long-term level in [Ziel \(2019\)](#), Figure 2 depicts the hourly load, the weekly and yearly moving average load in France and Germany. In both countries, the averaged load data exhibit gradual shifts in particular in the last four years, emphasizing their non-stationarity.

Our study deliberately bypasses formal unit root testing due to the ongoing research in this area, see e.g. [Schneider & Strielkowski \(2023\)](#), and the statistical complexities inherent in applying such tests to electricity time series. These complexities stem from the presence of structural breaks, non-linearities and seasonalities at various frequencies in the data, and potential small sample biases when aggregating data to long-term, e.g. annual, horizons. For a comprehensive assessment of unit root behavior in electricity time series, we recommend the literature reviews by [Schneider & Strielkowski \(2023\)](#); [Smyth \(2013\)](#).

2.2. Holiday Information

Holidays, of specific days or extended periods, significantly impact human behavior, often due to legal regulations. This usually leads to decreased work and industrial activity, consequently reducing electricity demand². This disruption to the typical weekly load pattern is evident in [Figure 3](#), which shows the load time series for the Easter and Christmas holiday time in Germany. Notably, the load profile of a holiday on a weekday, e.g. May 1st in 2015, frequently resembles that of a weekend.

Holiday information was collected from `Nager.Date`, see [Hager \(2024\)](#), is available from January 1st to December 31st of 2000 to 2030 and encompasses both the label and the day of occurrence of the holiday. These details undergo preprocessing, as described in [Chapter 3.4](#), to obtain holiday variables as a function of time. While holiday information is known in advance, making them deterministic information based on the calendar, their impact on load can be challenging to capture. This is due to their infrequent occurrence, usually once a year, making them a rare event in the context of load forecasting [Ziel \(2018\)](#); [Hong \(2010\)](#).

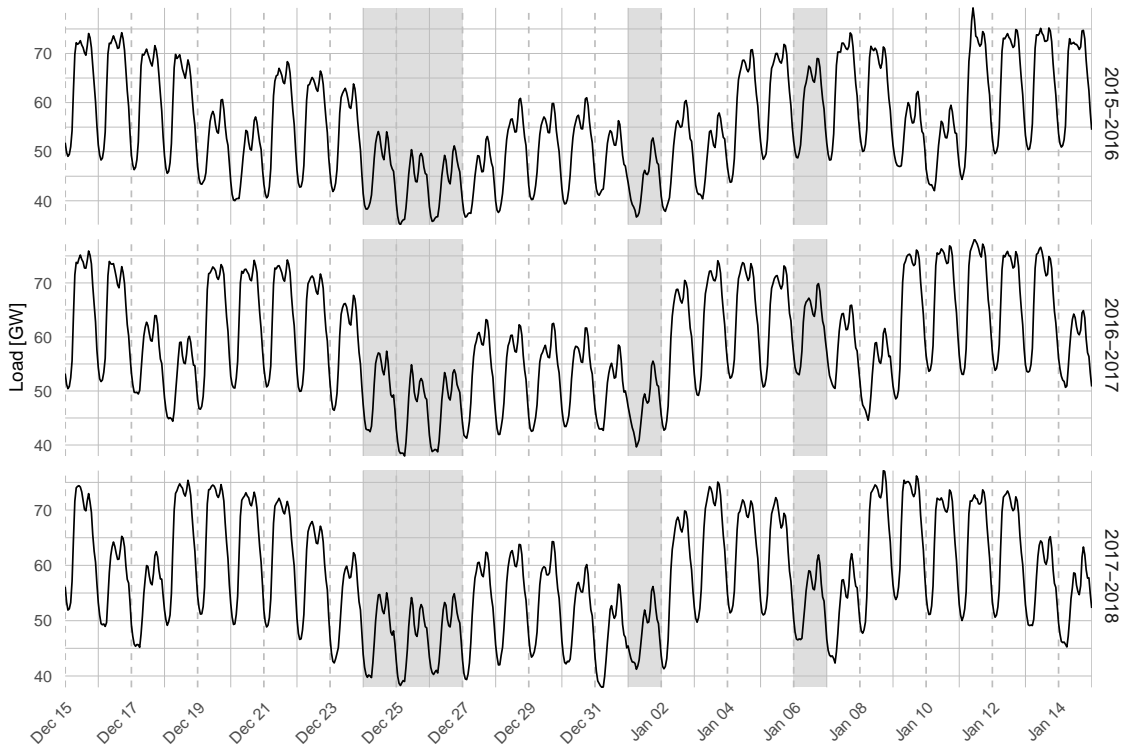
Two common holiday categories exist [Ziel \(2018\)](#); [Ziel & Liu \(2016\)](#); [Hong \(2010\)](#):

- Weekday holidays: These holidays occur annually on a specific weekday (e.g. Good Friday), but their date varies within the year. They usually exhibit a stable impact on load each year.
- Fixed-date holidays: These holidays occur on the same date every year (e.g. New Year’s Day), but the weekday on which they fall varies. They usually have a varying impact on load depending on the weekday on which they fall in a year.

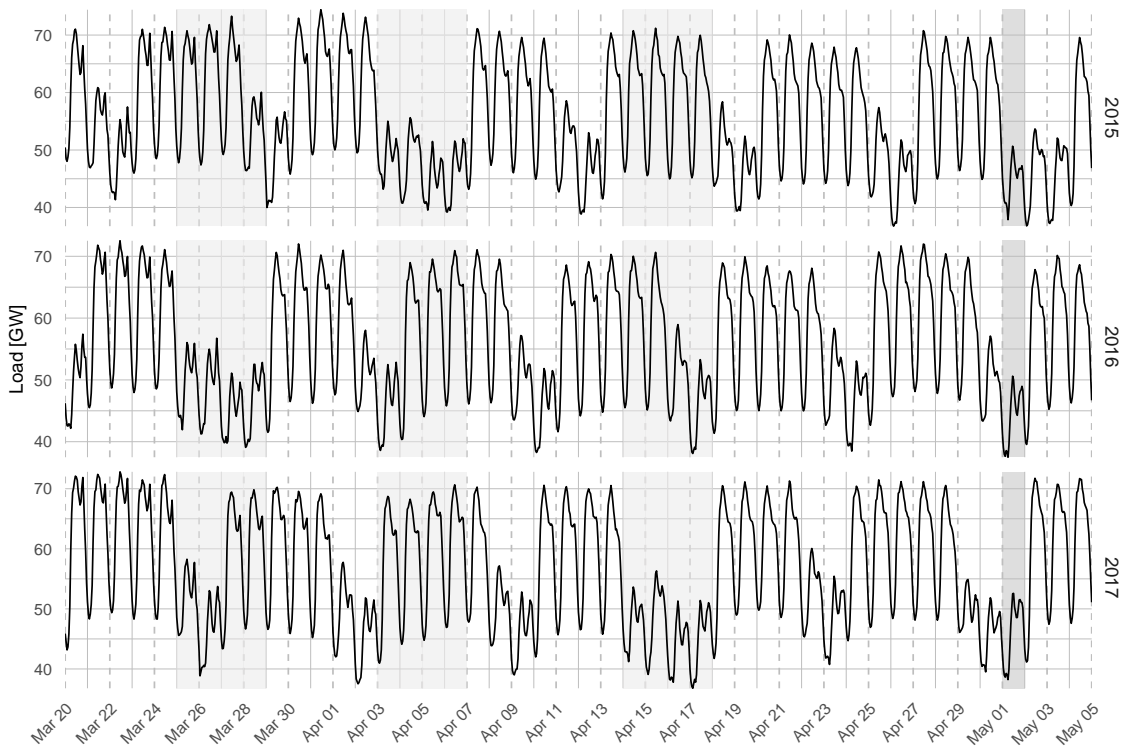
In addition to these single-day categories, we consider a winter holiday period encompassing December 18th to January 6th in every country.

[Figure 3](#) on load in the Easter and Christmas holiday time in Germany highlights the two distinct categories of single-day holidays. The Easter holidays Good Friday and Easter Monday have varying dates between late March and the middle of April. Their impact on load has remained consistent over the years. In contrast, the fixed-date holiday Labour Day on May 1st exhibits varying effects on load depending on the weekday it falls on. Notably, Labour Day on Sunday in 2016 resulted in negligible load reduction. The Christmas period is particularly evident, with a reduced load between Christmas and New Year’s Eve. For a similar [Figure](#) on load in France, we refer to [Figure 14](#) in [Appendix B](#). In France, the strong reliance of load on electric heating diminishes the visibility of holiday effects during the Christmas period.

²Note that areas with high tourism may experience increased demand during holidays.



(a) December 15th in 2015, 2016 and 2017 to January 15th in 2016, 2017 and 2018.



(b) March 1st to May 10th in 2016, 2017 and 2018.

Figure 3: Hourly load in Germany in the Easter and Christmas holiday time with holidays shaded in grey.

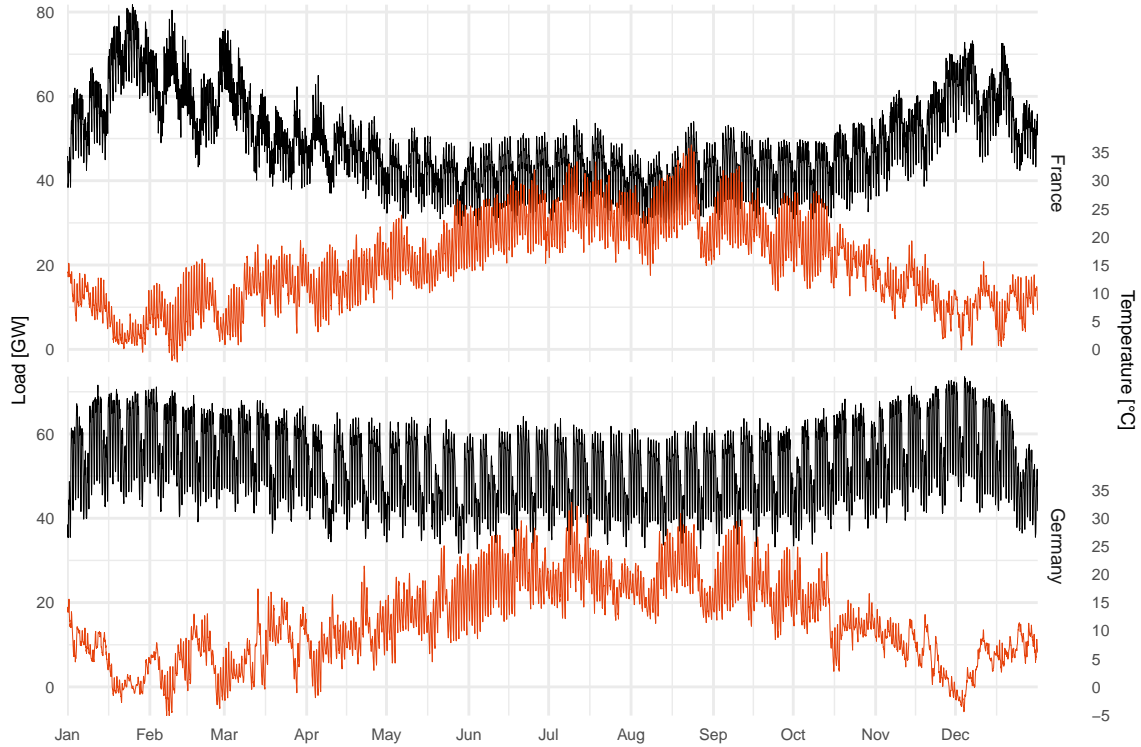


Figure 4: Hourly load (black) and temperature (red) in 2023.

2.3. Temperature

Hourly temperature observations are collected for each considered country from DWD ([Deutscher Wetterdienst \(2024\)](#)) starting from January 1st, 2015, to February 17th, 2024, at weather stations located in the most populous cities within each country. As load data, these temperatures exhibit clear seasonal patterns, including weekly and annual cycles, see Figure 4 on load and temperatures in France and Germany.

The non-linear relationship between temperature and load has been confirmed through various studies, see e.g. the overview by [Verwiebe et al. \(2021\)](#); [Davis et al. \(2016\)](#) and the comprehensive European study by [Bessec & Fouquau \(2008\)](#) or [Bashiri Behmiri et al. \(2023\)](#); [Ziel \(2018\)](#); [Xie et al. \(2018\)](#) among others. During summer when temperatures increase, load typically rises due to cooling demands. Conversely, during winter when temperatures fall, load increases in countries where electric heating is prevalent due to heating demands. As our model aims to encompass data from a diverse range of European nations, including countries with pronounced electric heating and cooling, like France, Spain and Italy, among others, factoring in temperature becomes essential for accurate load forecasting. For illustration, Figures 4 and 5 show the high sensitivity and non-linear relationship of load to temperature in France compared to a low sensitivity in Germany.

2.4. Countries

The data described above were initially gathered for all European countries participating in ENTSOE. However, certain countries had to be excluded due to data quality concerns, such as more than 5% missing load data, unavailability of day-ahead load or weather data, or more than 5 blocks of consecutive zeros in

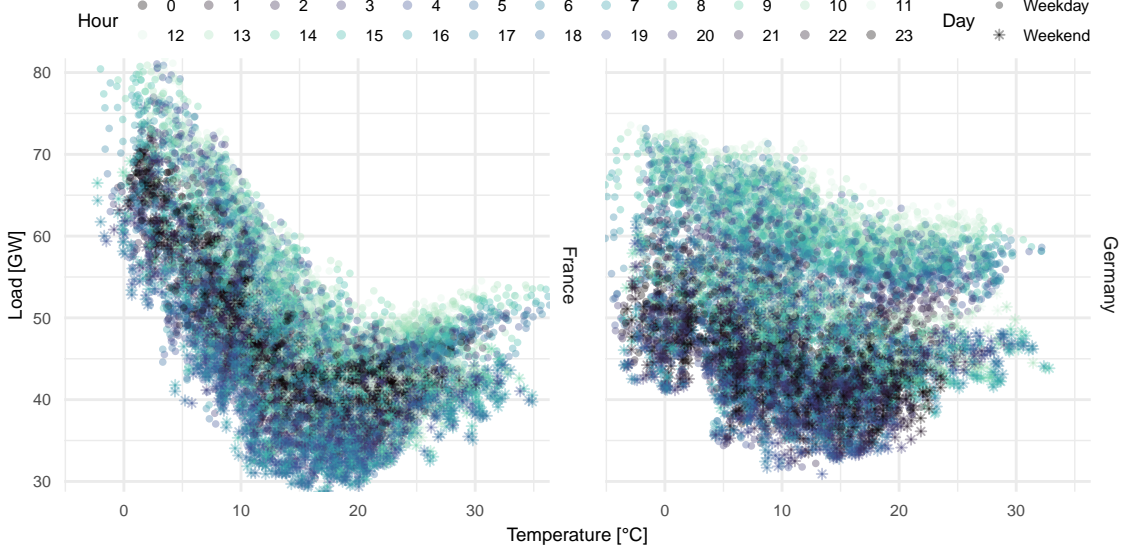


Figure 5: Temperature vs. hourly load in 2023.

reported load. This resulted in a final dataset encompassing data from 24 European countries: Austria, Belgium, Bulgaria, Czech Republic, Germany, Denmark, Estonia, Spain, Finland, France, Greece, Hungary, Italy, Lithuania, Latvia, Montenegro, Netherlands, Poland, Portugal, Romania, Serbia, Sweden, Slovenia, Slovakia. The average load of these countries in 2023 is illustrated by the Map 1. The figures in this and the subsequent chapters focus on France and Germany, as they are among the countries with the largest electricity demand and exhibit notable differences, e.g. in their dependence of load on temperature.

3. Methodology

3.1. Generalized Additive Models

Generalized Additive Models (GAM) are the main building blocks to capture the multifaceted characteristics of load in our proposed forecasting model. A GAM describes a response variable Y_t as an additive combination μ of smooth functions in covariates $\mathbf{X}_t = (X_t^1, \dots, X_t^m) \in \mathbb{R}^m$, $t \in \{1, \dots, N\}$. More precisely, there are smooth functions $f_i : \mathbb{R}^m \rightarrow \mathbb{R}$ in the covariates \mathbf{X}_t such that

$$Y_t = \mu(\mathbf{X}_t) + \varepsilon_t, \quad \mu(\mathbf{X}_t) = f_1(\mathbf{X}_t) + f_2(\mathbf{X}_t) + \dots + f_M(\mathbf{X}_t) \quad (1)$$

for ε_t independently and identically normally distributed random variables with zero mean. The objective to estimate in (1) is μ or the smooth functions³ f_1, \dots, f_M , respectively. Though in general, these smooth functions are arbitrary, we consider their marginals to lie in the k_1, \dots, k_m -rank spans of d -degree

³Note that smooth functions f_1, \dots, f_M can only be identified and thus estimated in (1) up to a constant. Consequently, practical applications employ identifiability constraints, commonly $f_i(\mathbf{X}_1) + \dots + f_i(\mathbf{X}_N) = 0$ or $f_i(0) = 0$, see Wood (2006) for details.

polynomial spline basis functions $\{b_1^1, \dots, b_{k_1}^1\}, \dots, \{b_1^m, \dots, b_{k_m}^m\}$:

$$f(x^1, \dots, x^m) = \sum_{i=1}^{k_1} \dots \sum_{j=1}^{k_m} \beta_{i, \dots, j} b_i^1(x^1) \cdot \dots \cdot b_j^m(x^m). \quad (2)$$

The resulting curve $f : \mathbb{R}^m \rightarrow \mathbb{R}$ becomes a spline of degree d if the basis functions are joined together at a m -dimensional grid of knots $\{x_1^1, \dots, x_{n_1}^1\} \times \dots \times \{x_1^m, \dots, x_{n_m}^m\}$ such that f has finite support $[x_1^1, x_{n_1}^1] \times \dots \times [x_1^m, x_{n_m}^m]$ and $f \in \mathcal{C}^2$. Representation (2) of a smooth function f as a linear combination of the products of basis functions, allows the application of linear estimation methods, such as an ordinary least squares estimation on the evaluation of basis functions. The model matrix \mathbb{X} in this case has rows of the form $\mathbb{X}_t = (\mathbb{X}_{t,1}^1 \otimes \dots \otimes \mathbb{X}_{t,m}^1, \dots, \mathbb{X}_{t,1}^M \otimes \dots \otimes \mathbb{X}_{t,m}^M)$ for the tensor product \otimes on matrix space and $\mathbb{X}_{t,j}^l = (b_1^j(X_t^j), \dots, b_{k_j}^j(X_t^j))$ evaluating the marginal bases of the smooth term f_l in covariate X^j at time $t \in \{1, \dots, N\}$. Among various polynomial spline bases, the B-spline basis is particularly common, see [Eilers & Marx \(2021\)](#).

To smooth the terms f_1, \dots, f_M in (1) a penalized least-squares objective with smoothing parameters $\lambda_i \in \mathbb{R}_{\geq 0}^m$ is applied:

$$\|\mathbf{Y} - \mathbb{X}\boldsymbol{\beta}\|^2 + \sum_{i=1}^M \lambda_i \mathcal{P}(f_i). \quad (3)$$

Consequently, the smoothing parameters λ_i balance an optimal model fit, achieved by low values of λ_i , and high levels of smoothness, achieved by high values of λ_i . In the case of B-splines, [Eilers & Marx \(2021\)](#) introduced a difference-based penalty. Specifically, they penalize the deviation in parameters β_i for equidistant knot spacing:

$$\mathcal{P}\left(\sum_{i=1}^k \beta_i b_i(x)\right) = \sum_{i=1}^{k-p} (\Delta^p \beta_i)^2 = \boldsymbol{\beta}^T \mathbf{S} \boldsymbol{\beta}, \quad (4)$$

for a one-dimensional term, where Δ is the difference operator. The resulting smooth terms are named *P-splines*. For a so-called cyclic P-spline, terms are added to penalize deviation between the first and last coefficients, e.g. $(\beta_1 - 2\beta_n + \beta_{n-1})^2$ and $(\beta_2 - 2\beta_1 + \beta_n)^2$ for $p = 2$. The generalization of \mathcal{P} to multivariate splines sums the differences of parameters $\beta_{i, \dots, j}$ individually for each marginal, i.e. keeping all but one index fixed $\beta_{i, 1, \dots, 1}$ for $i \in \{1, \dots, k_1\}$. Applied to the penalized least-squares objective (3), each marginal difference of parameters receives an individual smoothing parameter, leading to an m -dimensional smoothing parameter $\lambda_i \in \mathbb{R}_{\geq 0}^m$ for each smooth term f_1, \dots, f_M .

To select appropriate parameters β_i and smoothing parameters λ_i , minimization of criteria such as the generalized cross-validation (GCV) score or the unbiased estimator criterion (UBRE), REML or ML estimation, and variations thereof can be applied. For further insights on these criteria and methods of minimization, we refer to [Wood \(2006\)](#) or [Lepore et al. \(2022\)](#). GAM modeling and estimation methods are implemented in the R-package `mgcv`, see [Wood \(2006\)](#).

3.2. Additive Autoregressive and State Models

To capture the effect on load by past observation two types of models, which generate forecasts as weighted sums of autoregressive and initial state components, are incorporated in our load forecasting model: Autoregressive (AR) and Error-Trend-Seasonal (ETS) Models.

AR _{AIC} ($\nu, \phi; p_{\max}$)	ETS(α)	ETS($\alpha, \gamma; m$)
$Y_t = \nu + \sum_{k=1}^p \phi_k Y_{t-k} + \epsilon_t$	$Y_t = l_{t-1} + \epsilon_t$	$Y_t = l_{t-1} + s_{t-m} + \epsilon_t$
$\hat{Y}_{t+h t} = \nu + \sum_{k=1}^p \phi_k \hat{Y}_{t+h-k t}$	$l_t = l_{t-1} + \alpha \epsilon_t$	$l_t = l_{t-1} + \alpha \epsilon_t$
$\hat{Y}_{t+h-k t} = Y_{t+h-k}$ for $h \leq k$	$\hat{Y}_{t+h t} = l_t$	$s_t = s_{t-m} + \gamma \epsilon_t$
		$\hat{Y}_{t+h t} = l_t + s_{t+h-m} \lceil \frac{h}{m} \rceil$

Table 1: AR model of AIC-selected order $p \in \{1, \dots, p_{\max}\}$, additive ETS models with level state l_t , seasonal state s_t , smoothing parameters $\alpha, \gamma \in (0, 1)$ and periodicity m for zero mean white noise ϵ_t with forecasting equations for $h = 1, 2, \dots$

For AR models (see Tab. 1, col. 1) the optimal autoregressive order p is chosen by minimizing Akaike information criterion (AIC) over $p = 1, \dots, p_{\max}$ and parameter estimation is carried out by the Burg method, see Brockwell & Davis (2016).

While for AR models no assumption is imposed on the weights assigned to past observations, additive ETS models (see Tab. 1, col. 2-3), formulated by Hyndman & Athanasopoulos (2018), impose exponentially diminishing weights. This is obtained by applying exponential smoothing with respect to the additive decomposition of a time-series y_t into its states, i.e. level l_t and seasonal s_t component⁴. From the model formulation, it directly follows that the states and thus y_t itself exhibit unit root behavior, i.e. by first-order and seasonal differencing a stationary white noise process remains, whose evolution is regulated by the smoothing parameters $\alpha, \gamma \in (0, 1)$.

For estimation, Svetunkov (2023) implemented different multistep loss-function approaches. Specifically, estimation by trace MAE minimizes the sum of the $1, \dots, h_{\text{ETS}}$ steps ahead in-sample MAEs:

$$\text{TMAE} = \sum_{j=1}^{h_{\text{ETS}}} \frac{1}{T - h_{\text{ETS}}} \sum_{t=1}^{T-h_{\text{ETS}}} |e_{t+j|t}| \quad (5)$$

3.3. Modelling Concept

As detailed in Chapter 2.1, accurately forecasting load is a challenging task due to its multifaceted characteristics. Load depends on deterministic information, i.e. the seasonalities of different periods and holidays, and is sensitive to temperature fluctuations. Moreover, it is influenced by past observations. Thus, autoregressive components and non-stationary components need to be incorporated into a forecasting model. To address these diverse characteristics, we propose a two-stage GAM model integrating ETS and AR models. The general process of the model is illustrated by the flowchart in Figure 6 and described in the subsequent.

Let $Y_t \in \mathbb{R}$ and $X_t^{\text{Temp}} \in \mathbb{R}$ be the electricity load and temperature at time t for $t \in \{1, \dots, T\}$, respectively. Additionally, we have access to deterministic information about seasonalities and holidays for the extended horizon $t \in \{1, \dots, T+H\}$. It is the objective to forecast load over a mid-term prediction horizon H of several weeks to one year, resulting in forecasts $\hat{Y}_{T+1}, \dots, \hat{Y}_{T+H}$.

(i) Temperature forecast: In a first step, see Figure 6 on the left-hand-side, the proposed model constructs temperature forecasts \hat{X}_t^{Temp} , $t \in \{T+1, \dots, T+H\}$ for the mid-term horizon H . Since

⁴In all ETS models considered in this work the trend component is assumed to be zero.

accurate weather and satellite imagery-based temperature forecasts are not feasible for mid-term horizons, we rely on deterministic seasonalities, i.e. the time of the day and the time of the year, as modeling inputs. Observed temperatures X_t^{Temp} , $t \in \{1, \dots, T\}$ are, first, preprocessed to a smoothed time series using an ETS model (see Tab. 1, col. 2) with fixed smoothing parameters. This removes fluctuations not capturable by deterministic seasonalities and creates more suitable inputs for the subsequent models to forecast temperature and load. A GAM model is, secondly, applied to the smoothed temperature. Recognizing the limitations of lagged components in GAMs for mid-term horizons, we employ an AR model on the residuals of this GAM. The forecasted temperature is obtained by summing the individual forecasts from both models. By this, we incorporate crucial short-term temporal dependencies while avoiding computationally expensive solutions, like multiple GAM estimations with differently recent lags.

- (ii) **States fit and forecast:** In a second step, see Figure 6 middle part, the proposed model constructs level and seasonal states fit and forecast. For this, firstly, load is modeled by a GAM from the smoothed temperatures obtained in (i) and deterministic seasonal and holiday information. Secondly, an ETS model (see Tab. 1, col. 3) with an annual seasonality is applied to this GAM's residuals and fitted states are retrieved. The forecasted states follow directly from these fits. For estimation of the ETS model, a loss function covering a multiple of the weekly period is chosen. By this, fluctuations occurring in a smaller period are smoothed and not mirrored by the fitted and forecasted states component, which is well-suited, particularly, in the context of mid-term forecasting.
- (iii) **Load forecast:** Lastly, see Figure 6 right-hand-side, load is forecasted. For this, load is modeled again by a GAM with the smoothed temperatures, seasonal and holiday information and, additionally, with the ETS unit root states, i.e. level and annual seasonal, information as inputs. By this, the unit root behavior of the load time series is captured and overfitting of the GAM inputs in (ii) to this non-stationarity is avoided. For the same rationale as in (i), autoregressive dependencies of the load time series are captured by a secondary AR model on the residuals. Finally, load is forecasted as the sum of these two model's forecasts with the temperature, level and seasonal forecasts obtained in (i) and (ii) and the deterministic seasonal and holiday information over the horizon.

3.4. Data Preprocessing

Utilizing temperature data $\text{Temp}_t \in \mathbb{R}$ observed at weather stations and time information $t \in 1, \dots, T$, variables $X_t^m \in \mathbb{R}$ of our GAM model are defined in Table 2 and described in the subsequent. As outlined in Chapter 2, our dataset encompasses hourly observations, resulting in $S = 24$ observations per day. Nevertheless, the methodology introduced in the subsequent chapters is formulated for arbitrary observations per day $S \in \mathbb{N}_{\geq 3}$, allowing the analysis of data collected at different resolutions. For instance, it can be applied to commonly observed half-hourly data for $S = 48$ or quarter-hourly data for $S = 96$. Without loss of generality, we assume that the time series begins on January 1st at 0 : 00.

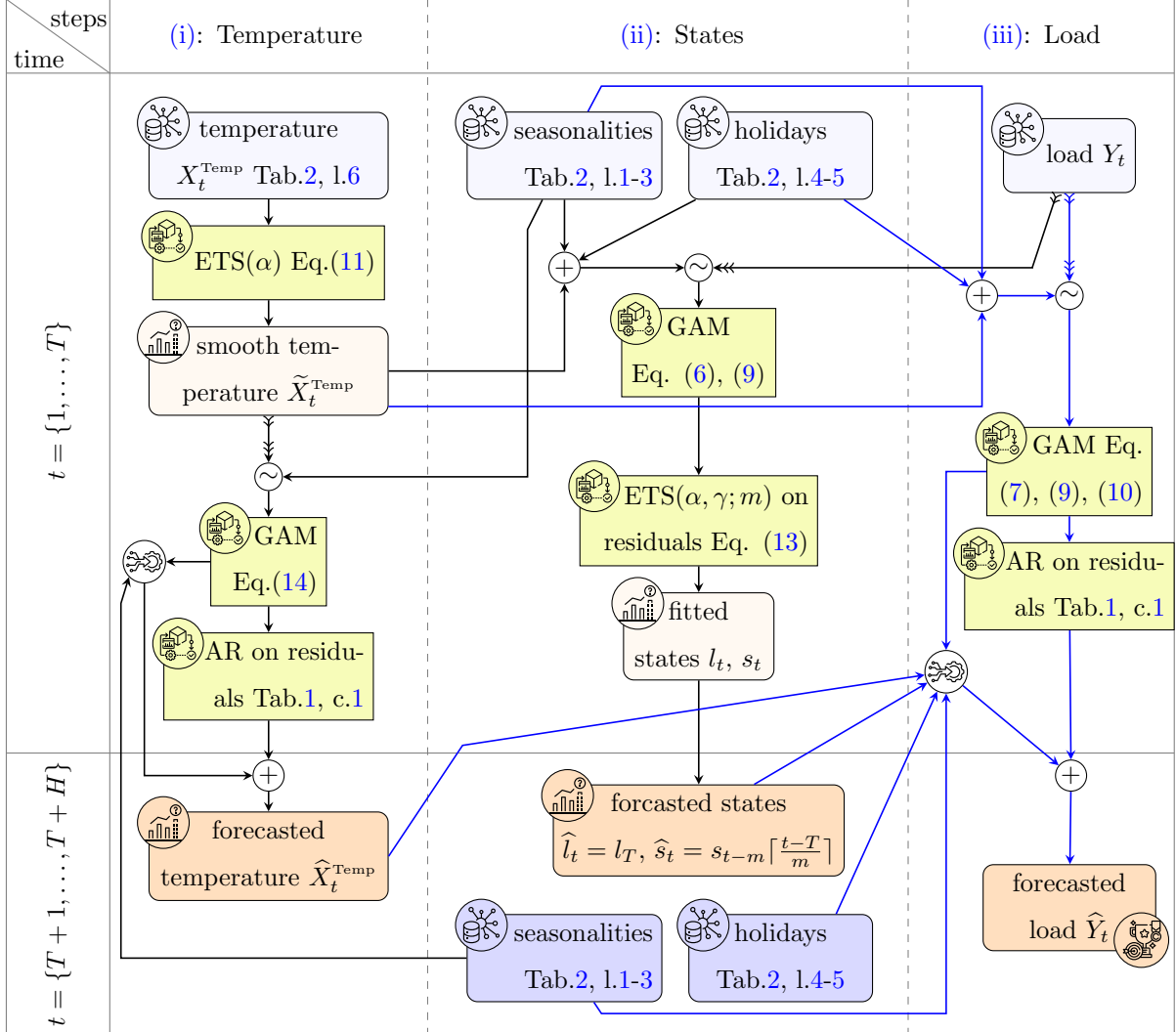


Figure 6: Flowchart representing the general process of the GAM model to forecast electricity load $\hat{Y}_{T+1}, \dots, \hat{Y}_{T+H}$. The external input information is framed by blue boxes and the output of models by orange boxes. Thereby, lighter shades are used for in-sample times and darker shades for out-of-sample times. Models are framed by yellow boxes. By blue lines, the inputs and models leading to the final load forecasts are marked.

The variable X_t^{HoY} is designed, to ensure a consistent representation of the time of the year across leap and non-leap years. This is guaranteed by a day of the year variable DoY_t adjusted for leap years. Specifically, the variable $\text{DoY}_t \in \{0, \dots, 364\}$ counts the day of the year starting with zero on January 1st and ending with 364 in non-leap years. If in a leap year, February 28th and 29th are assigned the same value of DoY_t . Subsequent values of DoY_t in the leap year have the same value, as in non-leap years.

The variable $X_{t_j}^{\text{HidP}}$ has discrete values in the set $\{0, 1, \dots, h_{\text{hldp}}\}$ representing the count of time steps from the beginning to the end of the holiday period. It is active only during the holiday period, taking the value zero otherwise. In the proposed model the holiday period starts on t_{hldp} set to December 18th at 0 : 00 and ends on January 6th at 23 : 00, covering $t_{\text{hldp}} = 20S$ hours.

Analogously to X_t^{HidP} , the variables of a weekday and fixed date holiday X_t^{HidW} and X_t^{HidF} have discrete values in the set $\{0, 1, \dots, 2b + S\}$ representing the holiday bridged to the previous and subsequent day by counting its time steps and being zero otherwise. Since holiday information is usually available only as the date of the holiday, preprocessing of this date to t_{hld} is necessary. In both GAM models, the smooth term in X_t^{HidF} will additionally be multiplied by an impact factor $X_{t_j}^{\text{Impact}}$ to account for the variation in the load reduction regarding the day of the week on which the holiday occurs.

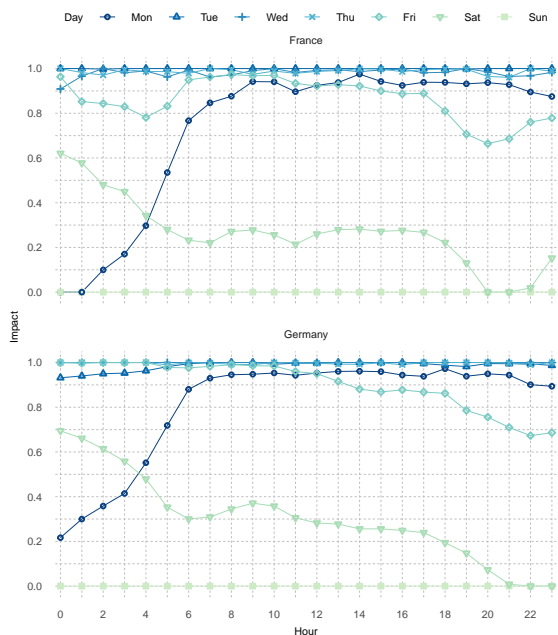


Figure 7: Evaluation of X_t^{Impact} for French and German hourly load data from January 1st, 2015 to December 31th, 2018.

Consequently, the multiplication of a smooth term in the fixed date holiday variable X_t^{HidF} with the impact variable $X_t^{\text{Impact}} = X_{t \bmod 7S}^{\text{Impact}}$ serves to eliminate the load effect if the holiday falls on a Sunday. Conversely, the impact is nearly maximal when the holiday falls on a Tuesday, Wednesday or Thursday. If the holiday falls on a Friday to Saturday, the impact is diminished.

The temperature variable X_t^{Temp} is calculated as the mean of temperatures Temp_t in $n_{\text{Temp}} = 5$ most

This impact factor, illustrated in Figure 7, is defined by the values of I_t bounded to $[0, 1]$. The numerator of I_t calculates the deviation of the weekly load profile, expressed as the median load for the hour $X_t^{\text{HoW}} \in \{0, \dots, 7S - 1\}$ of the week in the data, from the Sunday load profile, defined as the median load for the corresponding hour of the day on a Sunday $X_t^{\text{HoD}} + 6S \in \{6S, \dots, 7S - 1\}$ in the data. The denominator of I_t calculates the deviation from the peak weekly load profile, defined as the mean of the median loads for the corresponding hour of the day on Tuesday $X_t^{\text{HoD}} + S \in \{S, \dots, 2S - 1\}$, on a Wednesday $X_t^{\text{HoD}} + 2S \in \{2S, \dots, 3S - 1\}$ and on a Thursday $X_t^{\text{HoD}} + 3S \in \{3S, \dots, 4S - 1\}$ from the Sunday profile. Thus, the impact factor X_t^{Impact} provides an hourly ratio of the weekly load profile at time t to the peak weekly load profile scaled with respect to the Sunday load profile, which has an impact

Variable	Definition	Codomain
Hour of day	$X_t^{\text{HoD}} = t \bmod S$	$\{0, \dots, S - 1\}$
Hour of week	$X_t^{\text{HoW}} = t - t^* \bmod 7S$, where t^* is Monday at 0:00 in $\{1, \dots, 7S\}$.	$\{0, \dots, 7S - 1\}$
Hour of year	$X_t^{\text{HoY}} = \text{DoY}_t \times S + X_t^{\text{HoD}}$	$\{0, \dots, 365S - 1\}$
Holiday period	$X_t^{\text{HldP}} = \begin{cases} X_{t+1}^{\text{HoY}} - X_{t_{\text{hldp}}}^{\text{HoY}} & \text{for } t \in \{t_{\text{hldp}}, \dots, t_{\text{hldp}} + h_{\text{hldp}} - 1\} \\ 0 & \text{otherwise,} \end{cases}$ where $t_{\text{hldp}} \in \{1, \dots, T\}$ is the first occurrence of the holiday period of length h_{hldp} .	$\{0, 1, \dots, h_{\text{hldp}}\}$
Weekday and fixed date holiday	$X_t^{\text{Hld}} = \begin{cases} X_{t+1}^{\text{HoY}} - X_{t_{\text{hld}}-b}^{\text{HoY}} & \text{for } t \in \{t_{\text{hld}} - b, \dots, t_{\text{hld}} + b + S - 1\}, \\ 0 & \text{otherwise,} \end{cases}$ for $\text{hol} \in \{\text{HldW}, \text{HldF}\}$, where $t_{\text{hld}} \in \{1, \dots, T\}$ is the first occurrence of the weekday or fixed date holiday and $b \in \{0, \dots, S\}$ bridges the holiday to the previous and subsequent day by b time steps.	$\{0, 1, \dots, 2b + S\}$
Impact	$X_t^{\text{Impact}} = \min(\max(0, I_t), 1)$ $I_t = \frac{\text{med}(Y_{t^*} X_{t^*}^{\text{HoW}} = X_t^{\text{HoW}}) - \text{med}(Y_{t^*} X_{t^*}^{\text{HoW}} = X_t^{\text{HoD}} + 6S)}{\text{mean}(\text{med}(Y_{t^*} X_{t^*}^{\text{HoW}} = X_t^{\text{HoD}} + iS)_{i=1}^3) - \text{med}(Y_{t^*} X_{t^*}^{\text{HoW}} = X_t^{\text{HoD}} + 6S)}$	$[0, 1]$
Temperature	$X_t^{\text{Temp}} = \frac{1}{n_{\text{Temp}}} \sum_{i=1}^{n_{\text{Temp}}} \text{Temp}_t^i$	\mathbb{R}

Table 2: Definition of variables $X_t^m \in \mathbb{R}$ in the proposed two-stage GAM load forecasting model.

populated cities⁵ per country.

To preserve seasonal periodicities and account for a quick adjustment of human behavior to the local time, we adjust for daylight saving time changes in all variables except the meteorological temperature. Specifically, for all deterministic variables, clock change is considered non-existing. For the observed load data the missing hour in March is linearly interpolated and the double hour in October is averaged. The temperature variable X_t^{Temp} is defined in UTC, but adjusted in the same way, after ETS-smoothing and forecasting by the seasonal GAM.

Single outliers in the load data are handled via a lasso-based linear regression of load against a dummy for each observation, an Hour of the Day dummy and the running median of load for three consecutive observations. From the estimated λ -grid a model is chosen by squared BIC and the load time series is adjusted by the estimated observation dummies. Due to regression against the running median of three observations, only single outliers, but not consecutive outliers are detected. By including dummies for the hour of the day, the method takes the interday variation into account.

⁵Note that by this selection criterion, the cities used to calculate the average temperature may change over the study period. Additionally, note that various approaches exist to aggregate air temperatures per country. However, research by Neumann et al. (2023) and Sobhani et al. (2019) found no significant improvement over simple averaging compared to more sophisticated methods.

3.5. Model Specification

Our load forecasting model is composed of two stages of GAM models in sums of smooth terms μ_1 and $\mu_1 + \mu_2$, respectively, and an AR process on the second-stage residuals \mathcal{E}_t :

$$Y_t = v + \mu_1(\mathbf{X}_t) + \varepsilon_t, \quad (6)$$

$$Y_t = o + \underbrace{\mu_1(\mathbf{X}_t) + \mu_2(\mathbf{X}_t)}_{\text{smooth effects in the covariates}} + \underbrace{\mathcal{E}_t}_{\text{autoregressive effects}}, \quad (7)$$

$$\mathcal{E}_t = \nu + \phi_1 \mathcal{E}_{t-1} + \dots + \phi_p \mathcal{E}_{t-p} + e_t, \quad (8)$$

where $v, o, \nu \in \mathbb{R}$.

The additive terms μ_1 and μ_2 in equations (6) and (7) are defined as

$$\begin{aligned} \mu_1(\mathbf{X}_t) = & \underbrace{f^{\text{Temp},1}(\tilde{X}_t^{\text{Temp},1}) + f^{\text{Temp},2}(\tilde{X}_t^{\text{Temp},2})}_{\text{temperature effects}} \quad (9) \\ & + \underbrace{f^{\text{HoD}}(X_t^{\text{HoD}}) + f^{\text{HoW}}(X_t^{\text{HoW}}) + f^{\text{HoY}}(X_t^{\text{HoY}})}_{\text{seasonal effects}} \\ & + \underbrace{f^{\text{HoY,HoD}}(X_t^{\text{HoY}}, X_t^{\text{HoD}}) + f^{\text{HoY,HoW}}(X_t^{\text{HoY}}, X_t^{\text{HoW}})}_{\text{seasonal interaction effects}} \\ & + \underbrace{f^{\text{HidW}}(X_t^{\text{HidW}}) + X_t^{\text{Impact}} f^{\text{HidF}}(X_t^{\text{HidF}}) + f^{\text{HidP}}(X_t^{\text{HidP}})}_{\text{holiday effects}}, \\ \mu_2(\mathbf{X}_t) = & \underbrace{X_t^{\text{Level}} f^{\text{Level}}(X_t^{\text{HoD}}) + X_t^{\text{Season}} f^{\text{Season}}(X_t^{\text{HoD}})}_{\text{mid-term states effects}} \quad (10) \end{aligned}$$

and $\tilde{X}_t^{\text{Temp},1,2}$ are the fitted values of

$$X_t^{\text{Temp},1,2} \sim \text{ETS}(\alpha_{1,2}) \quad (11)$$

for $\alpha_1 = 1/S$ and $\alpha_2 = 1/14S$. All smooth effects f^m in the covariates are constructed as degree three, thus cubic, P-splines.

The mid-term states, i.e. level and seasonal, covariates X_t^{Level} , X_t^{Season} in (10) are derived from the residual term ε_t of the first stage GAM model (6), which captures temperature, seasonal, and holiday effects. Since the model (6) does not capture a unit root, this information remains in ε_t .

An intuitive approach to extract the unit-root states from ε_t would be to estimate an ETS model on ε_t with the multiple prevailing seasonalities, i.e. daily, weekly and annual seasonalities. However, an hourly ETS model with multiple seasonalities and a descent lead time would result in unfeasibly high computational expenses.

To receive a computationally feasible option, we apply temporal aggregation such that the frequency of ε_t is reduced to a weekly interval. This approach decreases the computational costs by reducing the data frequency by a factor of $7S$ and by eliminating the daily and weekly seasonality in ETS estimation. Nonetheless, it retains the typical unit root behavior in load levels and the annual seasonality.

The temporal aggregation of ε_t is defined as its average across specific hours of the week given by the set C :

$$r_\tau = \frac{1}{|C|} \sum_{c \in C} \varepsilon_{7S(\tau-1)+c} \quad (12)$$

Specifically, we choose $C = \bigcup_{n=0}^4 \{8, \dots, 19\} + nS$ representing the hours from 8:00 to 19:00 for each working day of the week (Mon-Fri). This choice aligns with the peak load definition commonly used in European electricity markets for trading electricity futures.

An ETS model with annual seasonality is applied to this averaged noise (see Tab. 1, col. 3):

$$r_\tau \sim \text{ETS}(\alpha, \gamma; m = 52) \quad (13)$$

with smoothing parameters α and γ for level and seasonal component, respectively.

The level and seasonal covariate X_t^{Level} and, X_t^{Season} for all $t \in \{1, \dots, T\}$ result from linear interpolation of the level and seasonal component l_τ and s_τ of (13) with extended boundaries. Thus, $X_t^{\text{Level}} = l_{\tau_1}$ and $X_t^{\text{Level}} = l_{\tau_T}$ for $t < \min(C)$ and $t > \max(C) + 7S\tau_T$, respectively, and analogously for X_t^{Season} .

The information loss from temporal aggregation in (12), which leads to diminished daily and weekly variation of covariates X_t^{Level} and X_t^{Season} is mitigated by multiplication⁶ of both covariates with cyclic smooth terms in X_t^{HoD} . While theoretically, it would be preferable to multiply with a smooth term in X_t^{HoW} the computational complexity renders it impractical. Instead, a smooth term in X_t^{HoD} suffices to capture the relevant information.

For all covariates with periodic structure, thus for seasonal and holiday covariates, spline types are cyclic, see Table 3. By appropriate positioning of the first and last knot, this guarantees under penalization of parameter deviation that $f^m(X_{np_m}^m) \approx f^m(X_{(n+1)p_m}^m)$ for period length p_m of the covariate X^m , $m \in \{\text{HoD}, \text{HoW}, \text{HoY}, \text{HldW}, \text{HldF}, \text{HldP}\}$ and analogously $f^m(X_{np_{m_1}}^{m_1}, X_{np_{m_2}}^{m_2}) \approx f^m(X_{(n+1)p_{m_1}}^{m_1}, X_{(n+1)p_{m_2}}^{m_2})$ for period lengths $p_{m_{\{1,2\}}}$ of the covariates $X^{m_{\{1,2\}}}$, $(m_1, m_2) \in \{(\text{HoD}, \text{HoY}), (\text{HoW}, \text{HoY})\}$. Thus, while $X_{np_m}^m \ll X_{(n+1)p_m}^m$, e.g. $X_{(n+1)p_m}^m - X_{np_m}^m = 365S$ for $m = \text{HoY}$, the transition from one period of f^m to the subsequent is approximately seamless, as required by the application. By way of illustration, it would be unsuitable for the smooth term in the HoY variable to be disconnected at the end of the year.

In line with the discrete range of values of seasonal and holiday covariates their intermittent knots⁷ are set to discrete. The chosen hyperparameters for the smooth terms, i.e. the basis ranks, knots and spline type are listed in Table 3.

To emphasize, the novelties of our GAM modeling approach are:

- (i) The individual handling of effects induced by each holiday separately as a smooth term in a discrete activation⁸ variable. By sensibly specifying this activation variable, additionally, the load reduction

⁶We intentionally choose a multiplication with a smooth term in X_t^{HoD} instead of a full interaction, thus a two-dimensional smooth term in covariates X_t^{HoD} and X_t^{Level} or X_t^{Season} . This choice aims to prevent an additional time-varying effect besides the level and seasonal states effect on load. The additive effect of level and seasonal states on load was retrieved from the ETS model in (13), where the gradual variation of these effects is governed by the estimated smoothing parameters α and γ . Embedding the derived covariates X_t^{Level} and X_t^{Season} into smooth terms would allow for these effects to additionally vary according to the estimated smooth term. Consequently, an extra time-varying effect on load would be introduced, potentially overlaying, and thus hindering interpreting, the effect of unit root states.

⁷Note that the number of knots is determined by the basis dimension k_m . More precisely, the number of knots is $k_m + 1$ for cyclic splines. Moreover, recall that knots are spaced equidistant for the traditionally defined P-Splines. Consequently, the basis dimension k_m has to be a divisor of the period length.

⁸To guarantee that the non-active and active hours of these holidays are transferred to the smooth splines, their identifiability constraints are set to $f^m(0) = 0$.

Smooth Term	Basis Dimension	Knots	Spline Type
$f^{\text{Temp},\{1,2\}}(\tilde{X}_t^{\text{Temp},\{1,2\}})$	$k_{\text{Temp}} = 6$		non-cyclic
$f^{\text{Temp}}(X_t^{\text{HoD}})$	$k_{\text{HoD}} = S$	$\{0, \dots, S\}$	cyclic
$f^{\text{HoW}}(X_t^{\text{HoW}})$	$k_{\text{HoW}} = 7S$	$\{0, \dots, 7S\}$	cyclic
$f^{\text{HoY}}(X_t^{\text{HoY}})$	$k_{\text{HoY}} = 12$	$\{0, 365S/12, 365S/6, \dots, 365S\}$	cyclic
$f^{\text{HoY,HoD}}(X_t^{\text{HoY}}, X_t^{\text{HoD}})$	$(k_{\text{HoY}}, k_{\text{HoD}}) = (12, S/3)$	$\{0, 365S/12, 365S/6, \dots, 365S\} \times \{0, 3, 6, \dots, S\}$	cyclic
$f^{\text{HoY,HoW}}(X_t^{\text{HoY}}, X_t^{\text{HoW}})$	$(k_{\text{HoY}}, k_{\text{HoD}}) = (12, 7)$	$\{0, 365S/12, 365S/6, \dots, 365S\} \times \{0, S, 2S, \dots, 7S\}$	cyclic
$f^{\text{HldW}}(X_t^{\text{HldW}})$	$k_{\text{HldW}} = S/3$	$\{0, 6, 12, \dots, 2S\}$	cyclic
$f^{\text{HldF}}(X_t^{\text{HldF}})$	$k_{\text{HldF}} = S/3$	$\{0, 6, 12, \dots, 2S\}$	cyclic
$f^{\text{HldP}}(X_t^{\text{HldP}})$	$k_{\text{HldP}} = S/3$	$\{0, 60, 120, \dots, 20S\}$	cyclic
$f^{\text{Level}}(X_t^{\text{HoD}})$	$k_{\text{Level}} = S/3$	$\{0, 3, 6, \dots, S\}$	cyclic
$f^{\text{Season}}(X_t^{\text{HoD}})$	$k_{\text{Season}} = S/3$	$\{0, 3, 6, \dots, S\}$	cyclic

Table 3: Definition of covariates $X_t^m \in \mathbb{R}$ in the proposed two-stage GAM load forecasting model. For the non-cyclic smooth terms in temperatures knots were not specified but set according to the common method on knot spacing, see [Wood \(2006\)](#), within the range of the covariate.

on previous and subsequent days induced by holidays that occur each year on a Tuesday or Thursday, e.g. Ascension Day or Corpus Christi in Germany, are captured. This approach is applied similarly to the extended holiday period of the Christmas vacation time. Moreover, we dampen the influence of holidays with a fixed date depending on the weekday they occur. With this individual holiday modeling, we differ from conventional methods that model holidays by a single holiday or weekend dummy, see [Ziel \(2018\)](#), assigning all holidays the same effect on load.

- (ii) We leverage a P-Spline GAM to forecast mid-term ETS-smoothed temperatures exclusively by seasonal patterns. This approach addresses the data scarcity, regarding accurate weather and satellite-imagery information, for forecasting periods ranging from several weeks to a year.
- (iii) To account for the mid-term forecasting horizon and the entailing gradual change of equilibrium load due to economic or socioeconomic variations, we incorporate state components. These components are obtained by an ETS model on the residuals of the first-stage GAM and thus exhibit a persistent trend behavior.

3.6. Estimation and Forecasting

Both GAM models (see Eq. (6) and (7)) are estimated by fast REML, according to (3), where in all splines parameter deviation of degree two is penalized. We allow for shrinking smooth terms to zero⁹, and

⁹If this is not specified in the estimation process, smooth terms are shrunk to the null space of the penalty functional $\mathcal{P}(\cdot)$ (see Eq. (4)), i.e. the subspace of splines $f(x) = \sum_{i=1}^k \beta_i b_i(x)$ such that $\mathcal{P}(f) = 0$. For cyclic P-splines this is, regardless

reduce effective sample size to obtain smoother fits, in a BIC-like range, see [Wood et al. \(2015\)](#). The AR process $\mathcal{E}_t \sim \text{AR}_{\text{AIC}}(\nu, \phi; p_{\max})$ (see Eq. (8)) is estimated as specified in Chapter 3.2 with $p_{\max} = 8 \times 7S$. For estimation of the ETS model (see Eq. (13)) the trace MAE (see Eq. (5)) for a horizon h_{ETS} of two weeks is minimized.

For non-deterministic variables, i.e. for the smooth temperature, level and seasonal variables, forecasts for each step of the horizon H have to be obtained.

The smooth temperature forecasts $\widehat{X}_t^{\text{Temp}\{1,2\}}$, $t \in \{T+1, \dots, T+H\}$ result from, firstly, estimating the GAM model

$$\begin{aligned} \widetilde{X}_t^{\text{Temp}j} &= c^{\text{Temp}} + \sum_{i=1}^{k_{\text{HoD},1}} \beta_i^{\text{HoD}} b_i^{\text{HoD}}(X_t^{\text{HoD}}) + \sum_{i=1}^{k_{\text{HoY}}} \beta_i^{\text{HoY}} b_i^{\text{HoY}}(X_t^{\text{HoY}}) \\ &+ \sum_{j=1}^{k_{\text{HoY}}} \sum_{i=1}^{k_{\text{HoD},2}} \beta_{ji} b_i^{\text{HoD}}(X_t^{\text{HoD}}) b_j^{\text{HoY}}(X_t^{\text{HoY}}) + e_t \end{aligned} \quad (14)$$

with cyclic cubic P-Splines and $k_{\text{HoD}} \in \{S, S/3\}$, $k_{\text{HoY}} = 6$ by fast REML with degree two parameter deviation penalties (see Eq. (3)). Secondly, an AR-process is estimated to the residuals of (14) as specified in Chapter 3.2: $\widehat{e}_t \sim \text{AR}_{\text{AIC}}(\nu, \phi; p_{\max})$ with $p_{\max} = 7 \times 4 \times S$.

The level and seasonal states forecasts result by $\widehat{l}_t = l_T$ and $\widehat{s}_t = s_{t-m} \lceil \frac{t-T}{m} \rceil$, $t > T$ from the estimated ETS model (13).

3.7. Benchmark Models

Eighth benchmark models, alongside the proposed GAM model, will be jointly analyzed in a forecasting study described in Chapter 4. These include two seasonal random walk models with weekly and annual periods ([SRWW](#), [SRWA](#)) that involve no parameter estimation and serve as baselines for comparison, three variations of the widely referenced Vanilla Model due to [Hong \(2010\)](#); [Hong et al. \(2014\)](#): a deterministic variant with no temperature information ([VanDet](#)), a basic variant with actual temperature information ([VanBas](#)) and a variant with additional recent temperature information ([VanRec](#)), an Autoregressive Weekly Difference Model ([ARWD](#)) based on [Haben et al. \(2019\)](#), a combined ETS and Seasonal Random Walk Model with Seasonal and Trend decomposition using Loess ([STL](#)) from the forecast package [Hyndman & Athanasopoulos \(2018\)](#) and, lastly, a Feed Forward Neural Network ([FNN](#)) with one hidden layer and linear output, which resulted as best performing model in [Bashiri Behmiri et al. \(2023\)](#):

- **SRWW, SRWA:** $\widehat{Y}_t = Y_{t-m} \lceil \frac{t-T}{m} \rceil$, $t \in \{T+1, \dots, T+H\}$, $m \in \{7S, 365S\}$

- **VanRec:**

$$\begin{aligned} Y_t &= \beta_0 + \beta_1 X_t^{\text{Trend}} + \beta_2 X_t^{\text{Month}} + \beta_3 X_t^{\text{Week}} + \beta_4 X_t^{\text{Hour}} + \beta_5 X_t^{\text{Week}} X_t^{\text{Hour}} + p(X_t^{\text{Temp}}) \\ &+ p(\widetilde{X}_t^{\text{Temp}1}) + p(\widetilde{X}_t^{\text{Temp}2}) + \epsilon_t, \end{aligned} \quad (15)$$

of the polynomial and penalty degree, the one-dimensional space of constant polynomials. In the non-cyclic case, this is for the penalty degree p , regardless of the polynomial degree, the $(p-1)$ -degree polynomials.

where $X_t^{\text{Trend}} = t$ represents a linear trend, $\mathbf{X}_t^{\text{Month}}$, $\mathbf{X}_t^{\text{Week}}$, $\mathbf{X}_t^{\text{Hour}}$ are class variables for the month, weekday and hour at time $t \in \{1, \dots, T + H\}$, $\tilde{X}_t^{\text{Temp}i}$ are the fitted values of (11) and

$$p(x) = \beta_6 x + \beta_7 x^2 + \beta_8 x^3 + \mathbf{X}_t^{\text{Month}}(\beta_9 x + \beta_{10} x^2 + \beta_{11} x^3) + \mathbf{X}_t^{\text{Hour}}(\beta_{12} x + \beta_{13} x^2 + \beta_{14} x^3). \quad (16)$$

Modelling equations of **VanDet** and **VanBas** are obtained from (15) by $p(X_t^{\text{Temp}}) = p(\tilde{X}_t^{\text{Temp}1}) = p(\tilde{X}_t^{\text{Temp}2}) = 0$ and $p(\tilde{X}_t^{\text{Temp}1}) = p(\tilde{X}_t^{\text{Temp}2}) = 0$, respectively. The temperature forecasts $\hat{X}_t^{\text{Temp}1,2}$, $t \in \{T + 1, \dots, T + H\}$, see (14), from our proposed model are applied.

- **ARWD**: $Y_t - \mu_t \sim \text{AR}_{\text{AIC}}(\nu, \phi; p_{\max})$, where μ_t is the sample mean of load for each hour of the week and the AR process is estimated as specified in Chapter 3.2.
- For **STL**, daily, weekly, and annual seasonal periods are applied for the decomposition and forecasts are computed by seasonal random walks for the seasonal components and an AIC selected ETS model for the seasonally adjusted time series.
- **FNN**: $Y_t = v + \sum_{j=1}^{k_{\text{FNN}}} v_j g\left(\sum_{j=1}^m w_{ij} \mathbf{X}_t\right)$, where $\mathbf{X}_t = (\tilde{X}_t^{\text{Temp}1}, \tilde{X}_t^{\text{Temp}2}, X_t^{\text{HoD}}, X_t^{\text{HoW}}, X_t^{\text{HoY}}, X_t^{\text{HidP}}, X_t^{\text{HidW}}, X_t^{\text{HidF}})$ for $\tilde{X}_t^{\text{Temp}i}$ the fitted values of (11), $m = |\mathbf{X}_t|$, $k_{\text{FNN}} = m/2 + 1$ and sigmoid activation function $g(x) = 1/(1 + \exp^{-x})$.

We designed an assortment of benchmarks with models covering the most relevant features for mid-term load forecasting, i.e. daily, weekly and annual, autoregressive and temperature effects, that includes both common linear and non-linear modeling techniques, and, encompasses frequently applied benchmarks in load forecasting, such as the linear Vanilla models used in GEFCom2012 and 2017 [Davis et al. \(2014\)](#); [Hong et al. \(2019\)](#) and [Høverstad et al. \(2015\)](#); [Ziel & Liu \(2016\)](#); [Luo et al. \(2018\)](#); [Xie et al. \(2018\)](#).

Given the heterogeneous dataset including countries with significant electric heating and cooling, we considered it essential to include benchmark models capturing temperature effects. We do not include a benchmark model capturing holiday effects, since the impact of these effects on forecasting accuracy is assessed in Chapter 5 by a comparison of our GAM model with and without holiday effects. For a comprehensive forecasting study on holiday handling in load forecasting, we refer to [Ziel \(2018\)](#).

4. Forecasting Study and Evaluation Design

To evaluate the proposed GAM model we conducted a rolling window forecasting study on the benchmark models, see Chapter 3.7, and our GAM model successively leaving out one modeling component, considered a novelty, i.e. the smooth effects in the temperature (**\Temp**), the mid-term smooth effects in the level and seasonal component (**\States**) and, lastly, the smooth effects in all three categories of holidays (**\Hid**). For the study, more than 8 years of load data, from January 2015 to February 2024 were used. In-sample data in each forecasting experiment comprised 4 years of data. Recall that data are observed at hourly resolution, thus in-sample data comprises $4 \times 365 \times 24$ observations per experiment. With each forecasting experiment the window of in-sample observations is rolled forward by 24 hours,

whereby the first hour to forecast is always 9 a.m. The forecasting horizon is chosen as 52 weeks, i.e. $H = 168 \times 52$. Due to the high overlap of hourly forecasts for a horizon of 52 weeks, the forecasting experiments of a study are highly correlated. Consequently, $N = 100$ experiments are randomly sampled from the total number of approximately $1460 = 4 \times 365$ forecasting experiments. This corresponds to approximately one experiment every two weeks. The impact variable X_t^{Impact} is calculated with load data from the first in-sample window only.

We evaluate forecasting accuracy using the mean absolute error (MAE)¹⁰ in three distinct ways: Firstly, to gain a comprehensive understanding, $\text{MAE}(\hat{\mathcal{E}}_h) = 1/N \sum_{n=1}^N |Y_{T+h} - \hat{Y}_{T+h,n}|$ is averaged over all hours in the forecasting horizon $h = 1, \dots, H$. Secondly, the significance of a difference in the overall average MAE between two models is tested via the Diebold-Mariano (DM) test introduced by [Diebold & Mariano \(1994\)](#). Thirdly, to identify temporal variations, $\text{MAE}(\hat{\mathcal{E}}_h)$ is averaged over the weeks $\{1, \dots, 52\}$ in the one-year forecasting horizons $\{1, \dots, H\}$ and over the hours $\{1, \dots, 24\}$ in $\{1, \dots, H\}$.

5. Results and Discussion

5.1. Overall Performance

Regarding overall performance, see Table 4, all GAM-type models ([GAM](#), [HLD](#), [Temp](#), [States](#)) distinctly outperform all, but the [FNN](#), benchmark models in every country included in the study. The best-performing GAM model has superior performance when compared to the [FNN](#) across all countries. Notably, [SRWW](#) and all three vanilla benchmark models ([VanDet](#), [VanBas](#), [VanRec](#)) exhibit low forecasting accuracy. Similar deficiencies in forecasting accuracy of Vanilla benchmarks were observed by e.g. [Browell & Fasiolo \(2021\)](#) or [Ziel & Liu \(2016\)](#); [Gaillard et al. \(2016\)](#) in GEFCom2014, see [Hong et al. \(2016\)](#), and [Ziel \(2019\)](#) in GEFCom2017, see [Hong et al. \(2019\)](#). However, including actual temperatures and recency temperature effects, even when only forecasted by seasonality, improves Vanilla forecasting accuracy. Among the benchmark models, [FNN](#) performs best, followed by the simple [SRWA](#) and the [STL](#) model.

With performance in the range of the GAM models, [FNN](#) is a considerable competitor for mid-term load forecasting. However, while good in capturing the effect of the multifaceted characteristics of load it lacks interpretability¹¹ in these. From our GAM model we will infer an intuitive and detailed understanding of how different factors influence load across specific time frames in Chapter 5.6.

¹⁰As a reminder, a regression-type GAM model is designed to forecast the mean, making RMSE the appropriate error measure. However, MAE, optimal for median forecasts, is applied, since it is more robust and due to its intuitive interpretability common in this type of literature. For a comparison of overall performance, RMSE is considered additionally in Table 6 in Appendix B. We specifically do not consider mean absolute percentage error (MAPE), though also common in this type of literature, due to its widely acknowledged theoretical shortcomings, see [Goodwin & Lawton \(1999\)](#); [Fildes \(1992\)](#); [Hyndman & Athanasopoulos \(2018\)](#); [Franses \(2016\)](#). For more details on error measures, we refer to [Gneiting \(2009\)](#).

¹¹While with FNN models one can interpret the sensitivity of load to changes in input variables, see e.g. [Behm et al. \(2020\)](#), they fail to provide insight into how the model’s input factors contribute to the assembly of load over the forecasted time frame, as demonstrated in Figures 13 and 17.

	SRWW	SRWA	STL	VanDet	VanBas	VanRec	ARWD	FNN	GAM	\HLD	\Temp	\States	DA	TSO
Austria	0.865	0.448	0.494	1.071	1.009	1.005	0.627	0.37	0.373	0.409	0.396	0.336	0.332	
Belgium	0.958	0.559	0.58	1.058	1	0.987	0.726	0.497	0.457	0.48	0.483	0.435	–	
Bulgaria	1.072	0.321	0.386	0.638	0.52	0.509	0.577	0.282	0.292	0.282	0.281	0.243	0.134	
Czech Rep.	1.037	0.432	0.477	1.043	0.934	0.92	0.745	0.348	0.347	0.392	0.375	0.317	0.119	
Denmark	0.447	0.249	0.244	0.582	0.551	0.538	0.336	0.241	0.202	0.212	0.207	0.217	0.049	
Estonia	0.157	0.067	0.073	0.15	0.124	0.123	0.118	0.055	0.056	0.058	0.06	0.053	0.07	
Finland	1.555	0.732	0.683	1.172	0.71	0.719	1.208	0.578	0.539	0.546	0.578	0.534	0.169	
France	11.499	4.536	4.839	8.193	5.72	5.601	8.75	3.75	3.751	3.77	4.418	3.524	0.948	
Germany	5.635	3.339	3.336	7.978	7.787	7.682	4.16	2.768	2.381	2.713	2.494	2.406	2.089	
Greece	0.968	0.567	0.615	0.953	0.865	0.833	0.69	0.465	0.456	0.47	0.495	0.453	0.174	
Hungary	0.564	0.326	0.369	0.605	0.574	0.564	0.407	0.274	0.293	0.322	0.307	0.252	0.225	
Italy	3.984	2.44	3.129	6.303	6.23	6.127	2.658	2.113	2.167	2.514	2.382	1.859	0.674	
Latvia	0.085	0.05	0.05	0.128	0.12	0.119	0.067	0.045	0.036	0.039	0.038	0.04	0.02	
Lithuania	0.154	0.087	0.094	0.205	0.193	0.19	0.113	0.073	0.077	0.082	0.079	0.069	0.037	
Montenegro	0.067	0.042	0.041	0.068	0.063	0.058	0.051	0.039	0.037	0.037	0.041	0.037	0.024	
Netherlands	1.428	0.844	1.252	1.61	1.535	1.515	1.12	0.987	0.852	0.851	0.822	0.928	1.259	
Poland	1.884	1.083	1.187	2.688	2.633	2.603	1.289	0.814	0.812	0.992	0.845	0.713	0.532	
Portugal	0.57	0.325	0.425	0.854	0.856	0.834	0.39	0.287	0.315	0.333	0.333	0.25	0.158	
Romania	0.726	0.469	0.483	0.84	0.786	0.784	0.551	0.387	0.37	0.412	0.407	0.359	0.096	
Serbia	0.694	0.352	0.367	0.617	0.498	0.503	0.584	0.39	0.299	0.304	0.33	0.346	0.141	
Slovakia	0.364	0.247	0.208	0.403	0.374	0.375	0.279	0.202	0.173	0.185	0.185	0.179	0.076	
Slovenia	0.202	0.118	0.121	0.241	0.232	0.23	0.147	0.104	0.096	0.104	0.1	0.097	0.046	
Spain	2.752	1.688	2.059	3.682	3.634	3.542	2.004	1.606	1.548	1.715	1.631	1.485	0.309	
Sweden	3.289	1.169	1.237	2.507	1.526	1.52	2.491	0.932	0.924	0.943	0.984	0.915	0.404	
Sum	40.956	20.493	22.748	43.586	38.474	37.88	30.088	17.606	16.853	18.164	18.27	16.046	8.085	

Table 4: Forecasting accuracy in terms of $MAE(\widehat{\mathcal{E}}_h)$ in GW for $h = 1, \dots, 168 \times 52$ for 24 European countries. The color scheme transitioning from red to yellow and green indicates models ranging from low to high accuracy. The best model for each country is marked by bolt writing. Day-ahead forecasts of the TSO (grey) are considered for countries where less than 1% of forecasts are missing.

As detailed in Table 5, the **FNN** is also disadvantageous to our GAM models in terms of computation time. The **FNN**'s computation time could be decreased by providing appropriate inputs. Consequently, the proposed GAM model may be employed as a first step in a model ensemble with an FNN. With the effect of most characteristics, in particular the non-stationarity, addressed, an FNN can focus on remaining non-linearities in a rigorously reduced time. This, additionally, mitigates the risk of suboptimal solutions in FNN optimization. By way of illustration, model ensembling with a machine learning model on a GAM's residuals resulted in a 5% gain in model performance in the study of [Nedellec et al. \(2014\)](#) and is advised in [De Vilmares & Goude \(2022\)](#).

The good performance of the simple **SRWA** benchmark highlights the importance of accounting for annual seasonality in mid-term load forecasting. The proposed GAM model incorporates this by a smooth yearly seasonal term and the ETS-modelled seasonal component. Additionally, the model could potentially be improved by decomposing with regard to the yearly seasonal component as a first modeling step and modeling it separately by an SRWA or by incorporating yearly lags in addition to the current

lags limited by the boundary $p_{\max} = 8 \times 168$.

Since a direct comparison with the day-ahead TSO forecasts is not reasonable due to the different objectives of forecasting horizon, they are not colored according to the red-green color scheme. However, the low difference between our best-performing GAM model to the TSO forecasts (e.g. in Austria, Estonia, Germany, Hungary, Netherlands and Poland the DA TSO outperforms by less than 70%) highlights the good performance of our model and its applicability in the industry, most importantly for long-term production and maintenance planning.

Within the GAM models, `\States` achieves the lowest average MAE in most countries. In the second-highest number of countries, the `GAM` model incorporating all effects (holidays, temperature, and states) has the lowest average MAE.

We observe a similar picture of overall performance for the entire European market assessed based on the sum of errors across all considered countries, see Table 4 last line, as well as for the RMSE as metric, see Table 6 in Appendix B.

5.2. Performance of `GAM` vs. `\States`

Figure 8, depicting the error measure for each forecasting experiment in France and Germany, reveals that high overall errors in the `GAM` vs. the `\States` model originate from the springtime in 2020. During this time the load level suddenly and considerably decreased due to COVID-19. This jump in the load level is not adequately captured by state components with forecasts equal to the last (seasonal) fitted value, as theoretically justified for a unit root process. By incorporating this (seasonally) constant state forecasts in the GAM model (see Eq. (7), (10)), errors accumulate for each forecasting step throughout the horizon. These effects are not present in shorter horizon load forecasting where incorporating unit root behavior showed a consistent improvement, see e.g.

Pierrot & Goude (2011); Goude et al. (2014); Nedellec et al. (2014); Ziel (2019).

Nevertheless, we view the `GAM` model as the more appropriate choice, due to the presence of unit root behavior in the load time series. This behavior is indicated by the estimated smoothing parameters α and γ (see Eq. (13)). Across the forecasting experiments, the average values of α and γ ($\bar{\alpha} = 0.32$, $\bar{\gamma} = 0.037$ in France, $\bar{\alpha} = 0.36$, $\bar{\gamma} = 0.029$ in Germany) are different from zero. Since the ETS model nests a non-unit root model for smoothing parameters approximately zero, these findings strongly suggest the presence of a unit root in the load level and a weak unit root in the annual seasonal component.

A more rapid adaptation of the state components, i.e. the average load over a specific (periodic)

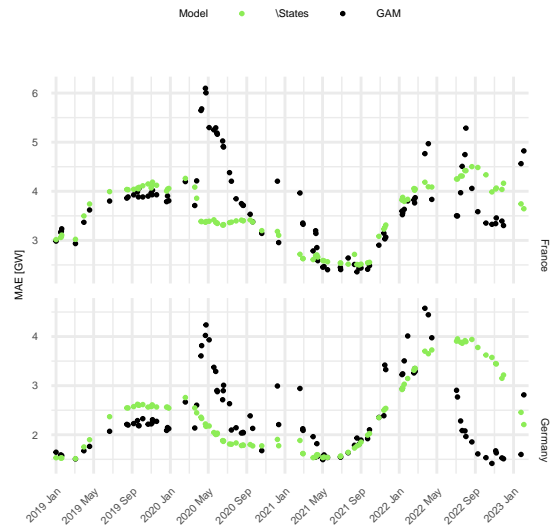


Figure 8: $MAE(\hat{\mathcal{E}}_n) = 1/H \sum_{h=1}^H |Y_{T+h} - \hat{Y}_{T+h,n}|$ in GW for $n = 1, \dots, N$.

timeframe, to shifted load values, could be achieved by shortening the corresponding timeframe. Specifically, in the proposed model this could be implemented by adjusting the horizon parameter $h_{ETS} = 2$ for loss minimization, and thus the estimated smoothing parameters α and γ (see Eq. (13)). However, firstly, as [Goude et al. \(2014\)](#) argue the load level represents a low-frequency effect and, secondly, as our model aims to capture mid-term unit root behavior suitable for a one-year forecasting horizon, further reduction of h_{ETS} is not considered appropriate. Moreover, we note that [Goude et al. \(2014\)](#) and [Nedellec et al. \(2014\)](#) improved accuracy by incorporating load levels on a monthly scale into their models. Thus, instead of decreasing h_{ETS} , increasing it could be considered.

Furthermore, to address exceptional periods, e.g. the COVID lockdown or energy crisis periods, our **GAM** model could be integrated in a state-space approach, as proposed by [De Vilmarest & Goude \(2022\)](#) and extended to a probabilistic forecasting model in [De Vilmarest et al. \(2024\)](#). In their study, which covered the COVID-19 period, [De Vilmarest & Goude \(2022\)](#) report that MAEs could nearly be halved through the adaptation of GAM parameters to different states using a generalization of the Kalman filter.

5.3. DM-Test Results

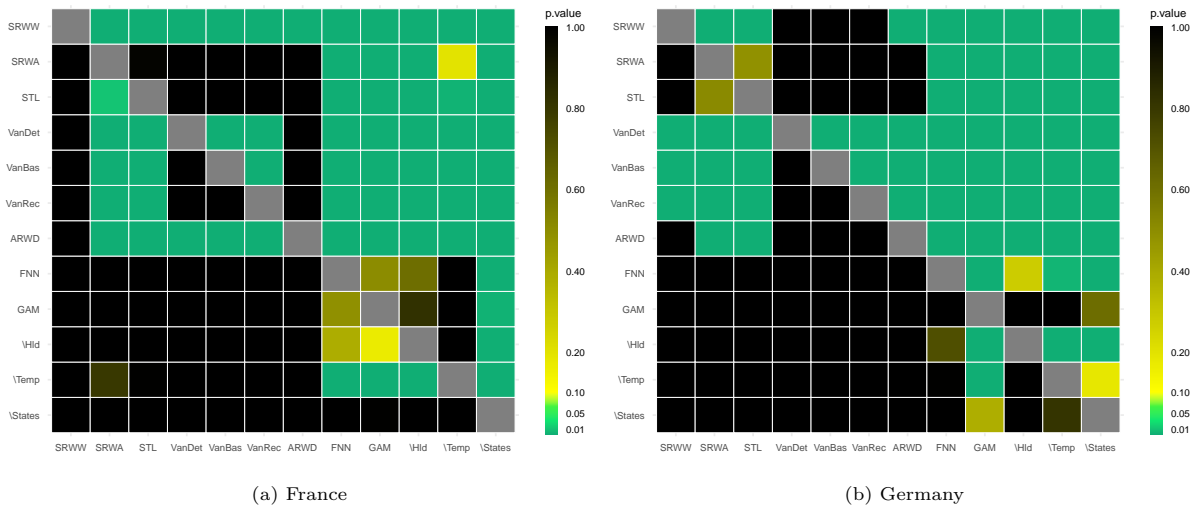


Figure 9: P-values of the DM-test for France and Germany.

Regarding the significance of the findings described in Chapter 5.1 for France and Germany, we observe from Figure 9 that including holiday and temperature effects improves accuracy significantly for Germany and France. Including mid-term state effects improved accuracy significantly only in Germany, whereas for the French load data, the GAM model including all but the states effect has significantly better forecasting accuracy compared to all other models.

For comparison, in the study by [Bashiri Behmiri et al. \(2023\)](#) on Italian load forecasts including temperature effects forecasted by random walk and climatological models¹² only showed significantly improved RMSE in a DM-test for short-term horizons. The divergent outcomes may be attributed to

¹²Specifically, [Bashiri Behmiri et al. \(2023\)](#) forecasts short-term (up to 7 days) daily temperatures by the last known daily averaged temperature and mid-term daily temperatures by the average daily temperature of the previous five years.

a different methodology in terms of integrating and modeling temperature. Whereas they integrate temperature as regressors in linear regression models comparable to **VanBas**, we model them by smooth terms. Additionally, their methodology lacks a daily variation, as they forecast daily averaged load from daily averaged temperatures. In contrast, the non-linear relation between load and temperature varies during the day as we see e.g. from Figure 5 and was observed by **Fan & Hyndman (2012)**. To emphasize, when true temperatures were incorporated instead of forecasts, a significant enhancement in accuracy, ranging from 10% to 20%, was observed. These values align closely with our findings (see Chapter ??),

However, when true temperatures were incorporated instead of forecasts, a significant enhancement in accuracy, ranging from 10% to 20%, was observed. These values align closely with our findings, indicating that the discrepancy may be attributed to the inaccuracies in their temperature forecasting.

Comparing the GAM-type models to benchmarks, except **FNN**, we fail to reject the null hypothesis of outperformance only for **\Temp**, which is surpassed by **SRWA** in France. This underscores the significance of integrating temperature effects in a country where electricity demand is influenced by heating and cooling.

When comparing the GAM-type models to the **FNN** benchmark, we observe a significantly better performance in France only for the **\States**, while in Germany, all GAM-type models, except for **\HLD**, exhibit significantly better performance. In the study by **Bashiri Behmiri et al. (2023)**, the similarly structured FNN model also outperformed regression-based models. However, the difference in RSME was significant only for a short-term horizon of up to one week. This diminished performance for the one-week horizon may be caused by the linearity of their regression-based models lacking variation in load throughout the week. Specifically, they use linear model structures that explain the weekly seasonality with dummies for Saturday, Sunday and Monday.

5.4. Weekly and Hourly Performance

For deeper insights, how MAE changes throughout the one-year forecasting horizons and the hours in one day, Figure 10 shows the weekly and hourly averaged MAEs for the three best-performing benchmarks and all GAM-type models in France and Germany.

We observe that models with autoregressive components (**STL** and GAM-type models) exhibit low initial errors that increase gradually as the forecast horizon extends. This effect is particularly visible in Germany. In France, a steep increase in errors within the first two weeks diminishes the visibility of the gradual increase in the mid-term. In comparison, the **SRWA** benchmark displays consistently high and middle-ranging errors across the horizon. This emphasizes the importance of autoregressive components for the short horizons and, in France a capturing of short-term weather effects by autoregressive components.

Comparing GAM-type models for a short-term horizon (up to 2 weeks) we observe in Germany, that the full **GAM** model and **\Temp** model perform best (approx. 15% and 7% better than **\HLD** and **\States**). In France, in particular, incorporating temperature effects contributes to improved forecasting accuracy (approx. 10% for horizons greater than a few days). This, along with the worse performance of the **STL** benchmark (approx. 15% and 60% in France and Germany, respectively) during this time frame

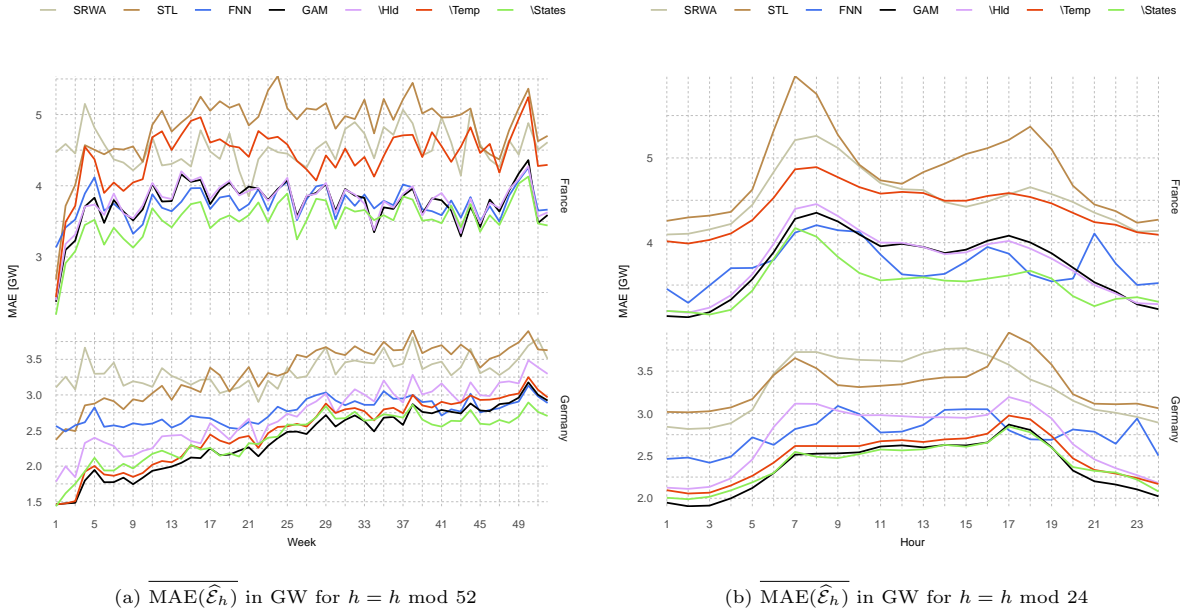


Figure 10: Mean MAE($\hat{\mathcal{E}}_h$) over weeks of the year and hours of the day for France and Germany.

highlights that capturing the multifaceted characteristics of load time series, and specifically factors affecting load on the mid-term, e.g. mid-term states components and holiday effects, improves performance not only in mid-term but also for short-term forecasting. Consequently, the proposed GAM-type models are also a suitable choice for short-term load forecasting.

The importance of these load characteristics varies between France and Germany. In France, we observe from comparing the different GAM-type models for the entire forecasting horizon, that the incorporation of temperature results in the most improvement in forecasting accuracy (approx. 20%), whereas including holiday effects has no observable effect. Conversely, in Germany, the inclusion of nuanced holiday smoothing terms brings the greatest improvement (approx. 10%), a value consistent with the findings of the comprehensive study conducted by Ziel (2018) on holiday handling in German load forecasting. In Germany, temperature effects only provide a minor enhancement (approx. 5%). This again highlights that particularly for countries with temperature-sensitive load profiles, including temperature information is beneficial even when accurate temperature forecasts are unavailable and models rely solely on seasonalities.

To enhance the effectiveness of our holiday handling in France, considering the introduction of a second holiday period could prove advantageous. As noted by Pierrot & Goude (2011), French load data typically exhibit a significant decline, particularly on weekdays, during August.

In order to achieve greater accuracy improvements through the inclusion of temperature effects in Germany, it may be beneficial to explore the most influential weather stations using GAM's GVC score, as proposed by Dordonnat et al. (2016). By this, regional disparities in electric heating and cooling patterns across Germany could be incorporated.

Regarding the change of performance for the different hours of the day, see Figure 10, we observe higher errors during peak demand hours (7-9 a.m., 5-7 p.m.) and lower errors during night and mid-

day hours of low demand for all models (approx. 25%, 15% for GAM-type models in France, Germany, respectively). Consequently, in further studies, multivariate models for high and low-demand hours, or in its most finely resolved form, for 24 hours as they are advocated in GAM load models by e.g. [Pierrot & Goude \(2011\)](#); [Nedellec et al. \(2014\)](#); [Dordonnat et al. \(2016\)](#); [Gaillard et al. \(2016\)](#), should be analyzed.

For the **FNN** benchmark, the error pattern for high- and low-demand hours is not clearly visible. In comparison to GAM-type models, **FNN** errors are particularly high for the early night hours and, in Germany, for the early morning hours. Again, this draws our attention to the potential of a model ensembling our proposed GAM model and an FNN. While the GAM model outperforms in capturing interday temporal dependencies with interpretable smooth terms in the variable X^{HOD} , a second-step FNN can address remaining non-linearities.

5.5. Computation Time

Computation times on a standard laptop are listed for France and Germany in Table 5.

While all benchmarks, except **FNN**, considered in this study performed significantly worse than the proposed GAM model, most of their computational times, of nearly under half a second are remarkably fast due to their simple linear structure. Note that a considerable amount of their computation time goes into outlier preprocessing, see Chapter 3.4. The computation time of the GAM models remains within a reasonable range, varying between 3.2 and 5.6 seconds. The computation time of the **FNN** benchmark is substantially higher when compared to the best-performing GAM model. However, when compared to more sophisticated machine learning models in load forecasting, our **FNN** still has low computation times. Other machine learning approaches for mid-term load forecasting e.g. deep neural networks used by [Han et al. \(2019\)](#) and model ensembles of machine learning approaches by [Li et al. \(2023\)](#) or [Agrawal et al. \(2018\)](#) took approximately half an hour to one hour for training.

	SRWW	SRWA	STL	VanDet	VanBas	VanRec	ARWD	FNN	GAM	\HLD	\Temp	\States
Time (FR)	0.06	0.06	1.00	0.05	0.05	0.06	0.54	6.70	5.55	4.07	5.00	3.33
Time (DE)	0.05	0.05	1.00	0.05	0.05	0.06	0.42	9.05	5.03	3.36	4.17	3.20

Table 5: Mean computation time of model estimation for France and Germany for $4 \times 365 \times 24$ observations on a standard laptop.

5.6. GAM Model Interpretation

To complement our analysis, Figure 11 demonstrates the holiday-specific load-reducing effect in France and Germany. The figure depicts the estimated smooth effects in (7) for weekday holidays (Good Friday, Easter Monday) and fixed day holidays (Labour Day, All Saints Day) fitted to the first in-sample data window of the forecasting study. Notably, the impact of Good Friday in France, a regional holiday celebrated by only approximately 5% of the population, is negligible. On the other hand, All Saints' Day, a regional holiday celebrated by roughly 57% of the German population, exhibits a weaker effect compared to non-regional holidays, but still a more pronounced effect than Good Friday in France. All non-regional holidays have a similar load-reducing effect. Load reduction is maximal around the first hours of the holiday and gradually decreases throughout the day, reaching a plateau or minimum level

by the late evening hours of the holiday. A similar load reduction profile is observed for most other holidays, which are depicted for France and Germany in Figures 16-15 in the Appendix B. From these Figures, we observe, that smooth terms in further holidays celebrated by a negligible percentage of the population, e.g. Abolition of Slavery (FR), Abolition de l'esclavage (FR)¹³, St. Stephen's Day (FR), International Women's Day (DE) World Children's Day (DE), and Repentance and Prayer Day (DE), are shrunk to zero, comparable to Good Friday in France. Note that the specification of the estimation method, see Chapter 3.6, allows for shrinking smooth terms to zero, instead of the null space. For our nuanced holiday modeling, this is particularly suitable and makes a pre-preprocessing of holiday data with an impact factor, according to their population share, obsolete.

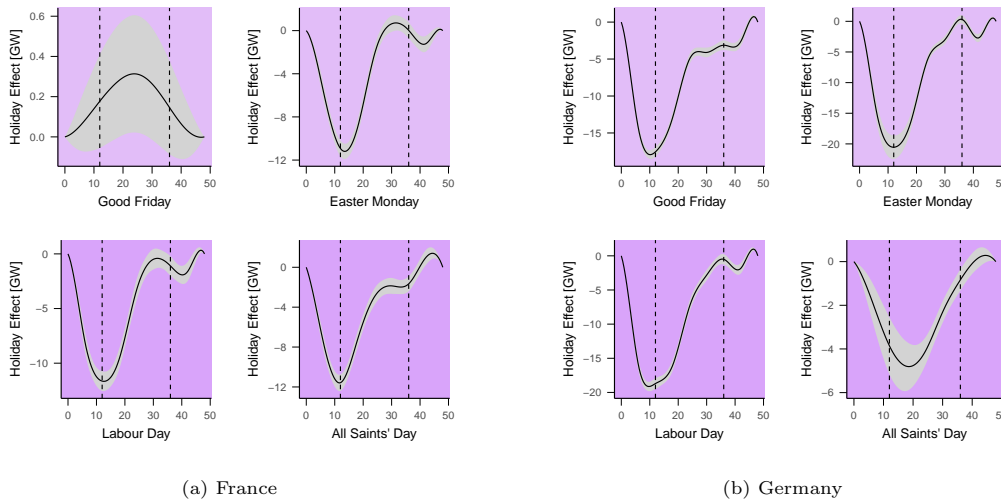


Figure 11: The smooth effects of bridged fixed day (purple) and weekday (light purple) holidays by (7) on load with dashed lines indicating the first and last hour of the holiday.

In addition to the effect induced by specific holidays, Figures 12 and 13 depict the effect induced by all load characteristics considered in our GAM model, see (7). The figures show the estimated smooth terms in holidays and the holiday period, seasonalities including interactions, temperature and mid-term states component fitted to the first in-sample data window of the forecasting study in the Christmas holiday time in France and the Easter holiday time in Germany, respectively. Furthermore, the fitted and actual loads reduced by the estimated intercept are pictured.

In France (Figure 12), as noted before, a clear temperature effect is observed with varying degrees from year to year (maximal load increase approx. 22 GW in 2016-2017, 12 GW in 2015-2016), whereas the effect of the states is minimal (maximal approx. 2 GW). The days where the effect of the Christmas holiday period (maximal load decrease approx. 5 GW) are active and non-active are distinctly visible. For the fixed-date holidays, we observe varying impacts, regarding the weekday of the holiday in the specific year (e.g. Christmas Day maximal load decrease approx. 13 GW (Fri) in 2015-2016, 0 GW (Sat) in 2016-2017, 13 GW (Mon) in 2017-2018). The effect of bridging the active hours of a holiday to the

¹³Abolition of Slavery and Abolition de l'esclavage, though having the same name, are different holidays in French overseas territories.

next day is particularly notable for the day after New Year’s Day (e.g. maximal load decrease approx. 5 GW in 2017-2018).

In Germany (Figure 13), consistent with previous observations, the impact of temperature is minimal (maximal approx. 2 GW). Similarly, the mid-term states exhibit a negligible effect within the depicted timeframes (maximal approx. 2 GW). Accordingly, on non-holidays seasonal effects, including their interactions, are the primary driver of the load profile with a typical daily and weekly pattern. For the fixed-date holiday Labour Day only a small bridged effect is observed in 2016, where the holiday occurs on a Sunday. In 2015 and 2017 this holiday has a load-reducing effect of approx. 17 GW.

Similar plots for the Easter holiday time in France and the Christmas holiday time in Germany can be found in the Appendix B, see Figures 18, 17.

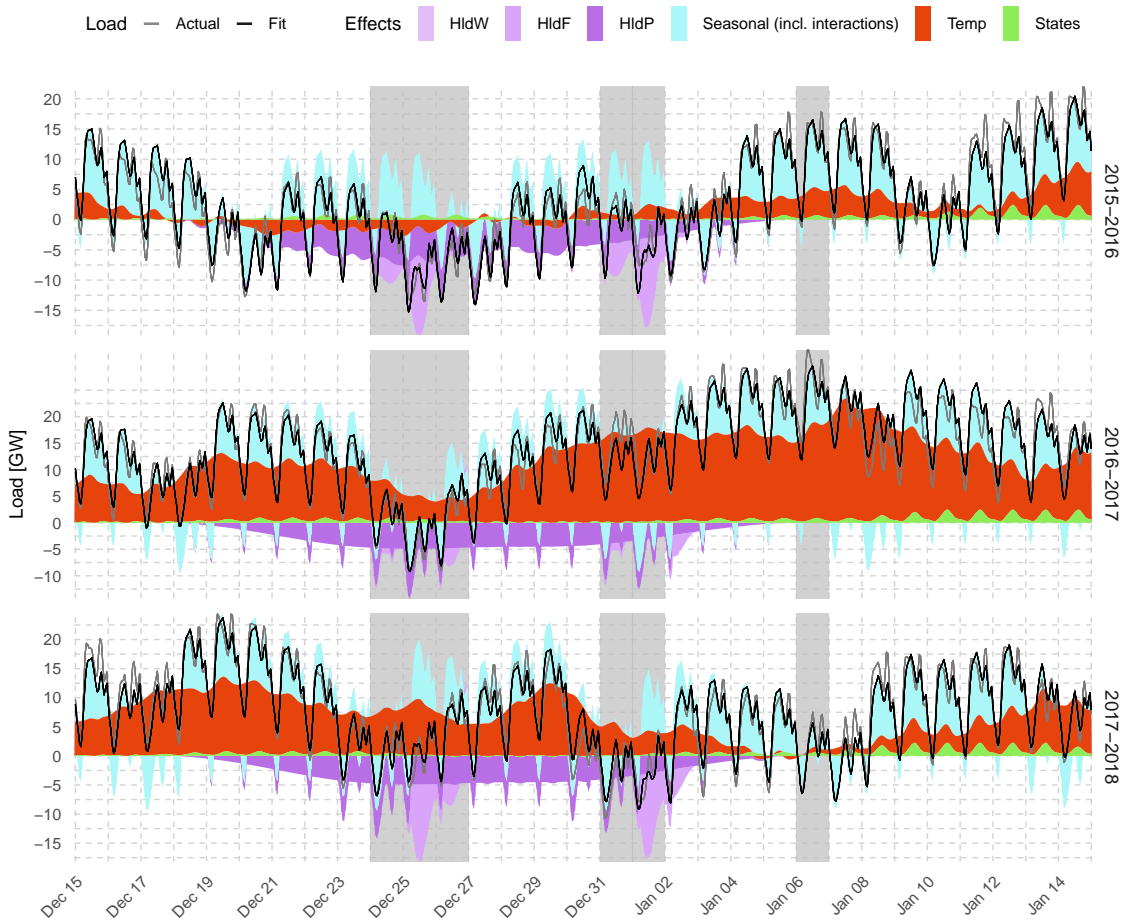


Figure 12: Estimated smooth effects, see (7), on load, fitted and actual load reduced by the estimated intercept in France from December 15th 2015, 2016 and 2017 to January 15th 2016, 2017 and 2018, with holidays shaded in grey.

6. Conclusion

This paper presents a novel, two-stage Generalized Additive Model (GAM) for effective, interpretable and robust mid-term hourly load forecasting across Europe. The model explicitly captures the multifaceted nature of load data by incorporating nuanced holiday modeling (vacation periods, fixed-day, and

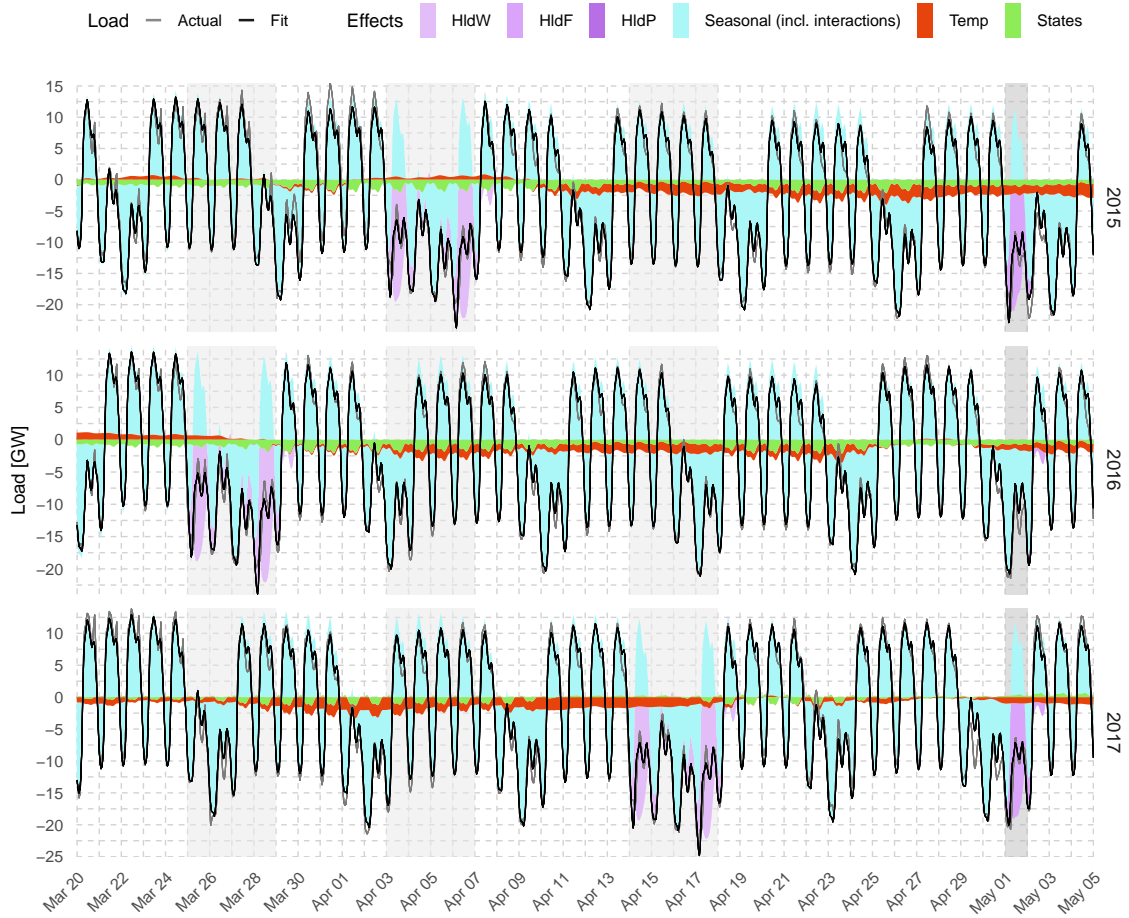


Figure 13: Estimated smooth effects, see (7), on load, fitted and actual load reduced by the estimated intercept in Germany from March 1st 2016, 2017 and 2018 to May 10th 2016, 2017 and 2018, with weekday holidays shaded in light grey and fixed date holidays shaded in dark grey.

weekday holiday effects) and exponentially smoothed temperatures, forecasted solely by seasonalities. These inclusions significantly improve forecasting accuracy, as demonstrated in an evaluation across 24 European countries over 9 years (2015-2024) of data. Accounting for the socio-economic characteristics in the load time series through an ETS-modeled mid-term load level and seasonal component yields ambiguous results across European countries. For countries that experienced a substantial load reduction during the COVID-19 pandemic, the incorporation of a mid-term level component reduces forecasting accuracy.

Beyond robust forecasting accuracy, our approach offers further advantages and resulting fields of application: Built as a linear model in interpretable P-splines, the model allows for understanding the impact of individual characteristics on load forecasts. Additionally, its linear structure enables remarkably fast computation times. These attributes, along with its significant improvements over standard linear models, make it a compelling candidate for model ensembling.

In future research, the proposed model may be employed in model ensembling with neural networks. While neural networks stand out at capturing non-linearities, interpretability, computational expense, and the risk of local solutions in optimization are a challenge. A pre-processed input in the form of our GAM model, with interpretability and most dependencies addressed, could allow a neural network to focus on remaining non-linearities while reducing computation time and the risk of suboptimal solutions.

Moreover, extensions of this paper will directly apply the proposed model for probabilistic trajectory forecasting. Generating load trajectories from our model is a straightforward process, as the model, constructed by independently estimated stages, encompasses independent noise distributions that allow for simulation.

Author Contributions

M. Z.: Conceptualization; methodology; software; validation; formal analysis; investigation; data curation; writing - original draft; writing review and editing; visualization.

F. Z.: Conceptualization; methodology; validation; formal analysis; funding acquisition; resources; writing - review and editing; supervision.

Funding Statement

This research has been funded by the Deutsche Forschungsgemeinschaft (DFG, German Research Foundation) – 505565850.

References

Agrawal, R. K., Muchahary, F., & Tripathi, M. M. (2018). Long term load forecasting with hourly predictions based on long-short-term-memory networks. In *2018 IEEE Texas Power and Energy Conference (TPEC)* (pp. 1–6). College Station, TX: IEEE. URL: <http://ieeexplore.ieee.org/document/8312088/>. doi:10.1109/TPEC.2018.8312088.

- Bashiri Behmiri, N., Fezzi, C., & Ravazzolo, F. (2023). Incorporating air temperature into mid-term electricity load forecasting models using time-series regressions and neural networks. *Energy*, *278*, 127831. URL: <https://share.goodnotes.com/s/XxP0y43YHDWre39ATwyXgV>. doi:10.1016/j.energy.2023.127831.
- Behm, C., Nolting, L., & Praktijnjo, A. (2020). How to model European electricity load profiles using artificial neural networks. *Applied Energy*, *277*, 115564. URL: <https://linkinghub.elsevier.com/retrieve/pii/S030626192031076X>. doi:10.1016/j.apenergy.2020.115564.
- Bessec, M., & Fouquau, J. (2008). The non-linear link between electricity consumption and temperature in Europe: A threshold panel approach. *Energy Economics*, *30*, 2705–2721. URL: <https://share.goodnotes.com/s/ChajSuLqvUhrSQwmaNelHO>. doi:10.1016/j.eneco.2008.02.003.
- Bouktif, S., Fiaz, A., Ouni, A., & Serhani, M. (2018). Optimal Deep Learning LSTM Model for Electric Load Forecasting using Feature Selection and Genetic Algorithm: Comparison with Machine Learning Approaches †. *Energies*, *11*, 1636. URL: <https://share.goodnotes.com/s/zAP0Fov3KF1DKjH7ADhWS4>. doi:10.3390/en11071636.
- Brockwell, P. J., & Davis, R. A. (2016). *Introduction to Time Series and Forecasting*. Springer Texts in Statistics. Cham: Springer International Publishing. URL: <https://share.goodnotes.com/s/NQEzjIz2SAzb8uAoDKd2o0>. doi:10.1007/978-3-319-29854-2.
- Browell, J., & Fasiolo, M. (2021). Probabilistic Forecasting of Regional Net-Load With Conditional Extremes and Gridded NWP. *IEEE Transactions on Smart Grid*, *12*, 5011–5019. URL: <https://ieeexplore.ieee.org/document/9520817/>. doi:10.1109/TSG.2021.3107159.
- Butt, F. M., Hussain, L., Jafri, S. H. M., Alshahrani, H. M., Al-Wesabi, F. N., Lone, K. J., Din, E. M. T. E., & Duhayyim, M. A. (2022). Intelligence based Accurate Medium and Long Term Load Forecasting System. *Applied Artificial Intelligence*, *36*, 2088452. URL: <https://www.tandfonline.com/doi/full/10.1080/08839514.2022.2088452>. doi:10.1080/08839514.2022.2088452.
- Chen, B., Chang, M., & Lin, C. J. (2004). Load Forecasting Using Support Vector Machines: A Study on EUNITE Competition 2001. *IEEE Transactions on Power Systems*, *19*, 1821–1830. URL: <https://share.goodnotes.com/s/wxYMqay0gVJEwSSZ3foxdS>. doi:10.1109/TPWRS.2004.835679.
- Davis, K. O., Hong, T., & Fan, S. (2016). Probabilistic electric load forecasting: A tutorial review. *International Journal of Forecasting*, *32*, 914–938. URL: <https://share.goodnotes.com/s/f47XjfMlIhndlVOD6uJiXx>. doi:10.1016/j.ijforecast.2015.11.011. MAG ID: 2275088575 S2ID: 154102a5a5e3a96fcd37bd5e672137126f323490.
- Davis, K. O., Hong, T., Pinson, P., & Fan, S. (2014). Global Energy Forecasting Competition 2012. *International Journal of Forecasting*, *30*, 357–363. URL: <https://share.goodnotes.com/s/GrKMTsCzqKjLsIKmqSvbF>. doi:10.1016/j.ijforecast.2013.07.001. MAG ID: 2081770709 S2ID: 9b1b1ee2c8761b5ac6c77ca3c7a34c184f154088.

- De Felice, M., Alessandri, A., & Catalano, F. (2015). Seasonal climate forecasts for medium-term electricity demand forecasting. *Applied Energy*, *137*, 435–444. URL: <https://linkinghub.elsevier.com/retrieve/pii/S030626191401071X>. doi:10.1016/j.apenergy.2014.10.030.
- De Vilmarest, J., Browell, J., Fasiolo, M., Goude, Y., & Wintenberger, O. (2024). Adaptive Probabilistic Forecasting of Electricity (Net-)Load. *IEEE Transactions on Power Systems*, *39*, 4154–4163. URL: <https://ieeexplore.ieee.org/document/10234679/>. doi:10.1109/TPWRS.2023.3310280.
- De Vilmarest, J., & Goude, Y. (2022). State-Space Models for Online Post-Covid Electricity Load Forecasting Competition. *IEEE Open Access Journal of Power and Energy*, *9*, 192–201. URL: <https://share.goodnotes.com/s/G0t88bwsURACzjy2boDi1H>. doi:10.1109/OAJPE.2022.3141883.
- Deutscher Wetterdienst (2024). Deutscher Wetterdienst - Bundesministeriums für Digitales und Verkehr. URL: https://www.dwd.de/DE/Home/home_node.html.
- Diebold, F. X., & Mariano, R. S. (1994). Comparing Predictive Accuracy. *Journal of Business & Economic Statistics*, . URL: <https://share.goodnotes.com/s/35y1Ry0qxtHXq117XGHScu>. doi:10.1198/073500102753410444. MAG ID: 2040503026 S2ID: 3405880c8faca87b2a500579d051930de26567c7.
- Dordonnat, V., Pichavant, A., & Pierrot, A. (2016). GEFCom2014 probabilistic electric load forecasting using time series and semi-parametric regression models. *International Journal of Forecasting*, *32*, 1005–1011. URL: <https://share.goodnotes.com/s/VC3wk1fkTKoXvccqczcfr>. doi:10.1016/j.ijforecast.2015.11.010.
- Eilers, P., & Marx, B. (2021). *Practical Smoothing: The Joys of P-splines*. Cambridge University Press. URL: <https://share.goodnotes.com/s/zVCX0FPXrXAXxVTc2uYo7q>.
- Fan, S., & Hyndman, R. J. (2012). Short-Term Load Forecasting Based on a Semi-Parametric Additive Model. *IEEE Transactions on Power Systems*, *27*, 134–141. URL: <https://share.goodnotes.com/s/s5QNJ49Z0GqxDf0tPkvciV>. doi:10.1109/TPWRS.2011.2162082.
- Fildes, R. (1992). The evaluation of extrapolative forecasting methods. *International Journal of Forecasting*, *8*, 81–98. URL: <https://share.goodnotes.com/s/UgfavmhYVP2Y20ApYFzz9w>. doi:10.1016/0169-2070(92)90009-X.
- Franses, P. H. (2016). A note on the Mean Absolute Scaled Error. *International Journal of Forecasting*, *32*, 20–22. URL: <https://share.goodnotes.com/s/7ycDkAcoJsxLdk7LjN5Efq>. doi:10.1016/j.ijforecast.2015.03.008.
- Gaillard, P., Goude, Y., & Nedellec, R. (2016). Additive models and robust aggregation for GEFCom2014 probabilistic electric load and electricity price forecasting. *International Journal of Forecasting*, *32*, 1038–1050. URL: <https://share.goodnotes.com/s/IVFD5r0F1QduwnTxvnsWXg>. doi:10.1016/j.ijforecast.2015.12.001. MAG ID: 2286305802 S2ID: 70f13938ddd85fc152302d6157d1deed2d11fc83.

- Ghiassi, M., Zimbra, D. K., & Saidane, H. (2006). Medium term system load forecasting with a dynamic artificial neural network model. *Electric Power Systems Research*, 76, 302–316. URL: <https://linkinghub.elsevier.com/retrieve/pii/S0378779605001951>. doi:10.1016/j.epsr.2005.06.010.
- Gil-Alaña, L., & Robinson, P. (1997). Testing of unit root and other nonstationary hypotheses in macroeconomic time series. *Journal of Econometrics*, 80, 241–268. URL: <https://share.goodnotes.com/s/onDIoqU2jWIrBV9QH5BoQi>. doi:10.1016/S0304-4076(97)00038-9.
- Gneiting, T. (2009). Making and Evaluating Point Forecasts. *arXiv: Statistics Theory*, . URL: <https://share.goodnotes.com/s/onDIoqU2jWIrBV9QH5BoQi>. doi:10.1198/jasa.2011.r10138. ARXIV_ID: 0912.0902 MAG ID: 2950861939 S2ID: 06f682919eafa8adbcc1b7bec23516cb962e7b22.
- Goodwin, P., & Lawton, R. (1999). On the asymmetry of the symmetric MAPE. *International Journal of Forecasting*, 15, 405–408. URL: <https://share.goodnotes.com/s/54XuT55qZ3UIzT10HlkagS>. doi:10.1016/S0169-2070(99)00007-2.
- Goude, Y., Nedellec, R., & Kong, N. (2014). Local Short and Middle Term Electricity Load Forecasting With Semi-Parametric Additive Models. *IEEE Transactions on Smart Grid*, 5, 440–446. URL: <https://share.goodnotes.com/s/54XuT55qZ3UIzT10HlkagS>. doi:10.1109/tsg.2013.2278425. MAG ID: 1991414280 S2ID: ebf703bad0082d55fbde21f6ef1dc1ed87e46d58.
- Haben, S., Georgios Giasemidis, Florian Ziel, & Siddharth Arora (2019). Short term load forecasting and the effect of temperature at the low voltage level. *International Journal of Forecasting*, 35. URL: <https://share.goodnotes.com/s/w09EGaWxgncYrSKcuMJ7R0>. doi:10.1016/j.ijforecast.2018.10.007. MAG ID: 2795649788 S2ID: aa22172da175eac60f7ae9ed41fdf701f8b6f607.
- Hager, T. (2024). Nager.Date. URL: <https://github.com/nager/Nager.Date>.
- Han, L., Peng, Y., Li, Y., Yong, B., Zhou, Q., & Shu, L. (2019). Enhanced Deep Networks for Short-Term and Medium-Term Load Forecasting. *IEEE Access*, 7, 4045–4055. URL: <https://share.goodnotes.com/s/zu7H8ZnJz5rBMvzF1BPagr>. doi:10.1109/ACCESS.2018.2888978.
- Harvey, A. C., Trimbur, T. M., & Van Dijk, H. K. (2007). Trends and cycles in economic time series: A Bayesian approach. *Journal of Econometrics*, 140, 618–649. URL: <https://share.goodnotes.com/s/LiQKMCQGJIbd7vORo1LMuq>. doi:10.1016/j.jeconom.2006.07.006.
- Hendry, D. F., & Juselius, K. (2000). Explaining Cointegration Analysis: Part II. *The Energy Journal*, 22, 75–120. URL: <https://share.goodnotes.com/s/cRpfcEscGu4FH43ck4vrix>. doi:10.5547/issn0195-6574-ej-vol22-no1-4. MAG ID: 2145978621 S2ID: 98ccf59c40a52d8746bf91b9d019528f060f1bf2.
- Hong, T. (2010). *Short Term Electric Load Forecasting*. Dissertation North Carolina State University.
- Hong, T., Pinson, P., Fan, S., Zareipour, H., Troccoli, A., & Hyndman, R. J. (2016). Probabilistic energy forecasting: Global Energy Forecasting Competition 2014 and beyond. *International Jour-*

- nal of Forecasting*, 32, 896–913. URL: <https://share.goodnotes.com/s/cRpfcEscGu4FH43ck4vrrix>. doi:10.1016/j.ijforecast.2016.02.001.
- Hong, T., Wilson, J., & Xie, J. (2014). Long Term Probabilistic Load Forecasting and Normalization With Hourly Information. *IEEE Transactions on Smart Grid*, 5, 456–462. URL: <https://share.goodnotes.com/s/cRpfcEscGu4FH43ck4vrrix>. doi:10.1109/TSG.2013.2274373.
- Hong, T., Xie, J., & Black, J. (2019). Global energy forecasting competition 2017: Hierarchical probabilistic load forecasting. *International Journal of Forecasting*, 35, 1389–1399. URL: <https://share.goodnotes.com/s/atNevIAR0xmwmM3Lbrcm6N>. doi:10.1016/j.ijforecast.2019.02.006.
- Hyndman, R. J., & Athanasopoulos, G. (2018). *Forecasting: principles and practice*. (2nd ed.). Lexington, Ky.: Otexts, online, open-access textbook.
- Høverstad, B. A., Langseth, H., Öztürk, P., & Tideman, A. (2015). Short-Term Load Forecasting With Seasonal Decomposition Using Evolution for Parameter Tuning. *IEEE Transactions on Smart Grid*, 6, 1904–1913. URL: <https://share.goodnotes.com/s/uP6WoNdpKy6wGCBsTSdKJ9>. doi:10.1109/tsg.2015.2395822. MAG ID: 1988725814.
- Kalhari, M. R. N., Emami, I. T., Fallahi, F., & Tabarzadi, M. (2022). A data-driven knowledge-based system with reasoning under uncertain evidence for regional long-term hourly load forecasting. *Applied Energy*, 314, 118975. URL: <https://linkinghub.elsevier.com/retrieve/pii/S0306261922003853>. doi:10.1016/j.apenergy.2022.118975.
- Lepore, A., Palumbo, B., & Poggi, J.-M. (Eds.) (2022). *Interpretability for Industry 4.0: statistical and machine learning approaches*. Cham: Springer. URL: <https://share.goodnotes.com/s/6f931DW9gJv47dPGah7DRF> oCLC: 1348479084.
- Li, D., Tan, Y., Zhang, Y., Miao, S., & He, S. (2023). Probabilistic forecasting method for mid-term hourly load time series based on an improved temporal fusion transformer model. *International Journal of Electrical Power & Energy Systems*, 146, 108743. URL: <https://linkinghub.elsevier.com/retrieve/pii/S0142061522007396>. doi:10.1016/j.ijepes.2022.108743.
- Luo, J., Davis, K. O., Hong, T., & Fang, S. (2018). Benchmarking robustness of load forecasting models under data integrity attacks. *International Journal of Forecasting*, 34, 89–104. URL: <https://share.goodnotes.com/s/0x9zN2ub4y2LdqHPhXedZR>. doi:10.1016/j.ijforecast.2017.08.004. MAG ID: 2763926615 S2ID: f8b553741997791fcb22668eba17f8baccf78519.
- Narayan, P. K., & Liu, R. (2015). A unit root model for trending time-series energy variables. *Energy Economics*, 50, 391–402. URL: <https://linkinghub.elsevier.com/retrieve/pii/S014098831400317X>. doi:10.1016/j.eneco.2014.11.021.
- Nedellec, R., Cugliari, J., & Goude, Y. (2014). GEFCom2012: Electric load forecasting and backcasting with semi-parametric models. *International Journal of Forecasting*, 30, 375–381. URL: <https://share.goodnotes.com/s/JlAtX2WFv0sUzpqVptGTUi>. doi:10.1016/j.ijforecast.2013.07.004.

- Nelson, C. R., & Plosser, C. R. (1982). Trends and random walks in macroeconomic time series. *Journal of Monetary Economics*, *10*, 139–162. URL: <https://linkinghub.elsevier.com/retrieve/pii/0304393282900125>. doi:10.1016/0304-3932(82)90012-5.
- Neumann, O., Turowski, M., Mikut, R., Hagemeyer, V., & Ludwig, N. (2023). Using weather data in energy time series forecasting: the benefit of input data transformations. *Energy Informatics*, *6*, 44. URL: <https://share.goodnotes.com/s/nXkWZUV3wEbH5j5M14mEWX>. doi:10.1186/s42162-023-00299-8.
- Oreshkin, B. N., Dudek, G., Pelka, P., & Turkina, E. (2021). N-BEATS neural network for mid-term electricity load forecasting. *Applied Energy*, *293*, 116918. URL: <https://linkinghub.elsevier.com/retrieve/pii/S0306261921003986>. doi:10.1016/j.apenergy.2021.116918.
- Perron, P. (1997). Further evidence on breaking trend functions in macroeconomic variables. *Journal of Econometrics*, *80*, 355–385. URL: <https://linkinghub.elsevier.com/retrieve/pii/S0304407697000493>. doi:10.1016/S0304-4076(97)00049-3.
- Petropoulos, F., Apiletti, D., Assimakopoulos, V., Babai, M. Z., Barrow, D. K., Taieb, S. B., Bergmeir, C., Bessa, R., Bijak, J., Boylan, J. E., Browell, J., Carnevale, C., Castle, J. L., Cirillo, P., Clements, M. P., Cordeiro, C., Oliveira, F. L. C., Baets, S. D., Dokumentov, A., Ellison, J., Fiszeder, P., Franses, P. H., Frazier, D. T., Gilliland, M., Gönül, M. S., Goodwin, P., Grossi, L., Grushka-Cockayne, Y., Guidolin, M., Gunter, U., Guo, X., Guseo, R., Harvey, N., Hendry, D. F., Hollyman, R., Januschowski, T., Jeon, J., Jose, V. R. R., Kang, Y., Koehler, A. B., Kolassa, S., Kourentzes, N., Leva, S., Li, F., Litsiou, K., Makridakis, S., Martin, G. M., Martinez, A. B., Meeran, S., Modis, T., Nikolopoulos, K., Önkal, D., Paccagnini, A., Panagiotelis, A., Panapakidis, I., Pavia, J. M., Pedio, M., Pedregal, D. J., Pinson, P., Ramos, P., Rapach, D. E., Reade, J. J., Rostami-Tabar, B., Rubaszek, M., Sermpinis, G., Shang, H. L., Spiliotis, E., Syntetos, A. A., Talagala, P. D., Talagala, T. S., Tashman, L., Thomakos, D., Thorarinsdottir, T., Todini, E., Arenas, J. R. T., Wang, X., Winkler, R. L., Yusupova, A., & Ziel, F. (2022). Forecasting: theory and practice. *International Journal of Forecasting*, *38*, 705–871. URL: <https://www.sciencedirect.com/science/article/pii/S0169207021001758>. doi:<https://doi.org/10.1016/j.ijforecast.2021.11.001>.
- Pierrot, A., & Goude, Y. (2011). Short-Term Electricity Load Forecasting With Generalized Additive Models. *2011*, . URL: <https://share.goodnotes.com/s/8REN6n7LjRRLWT8bBMMBF1>.
- Schneider, N., & Strielkowski, W. (2023). Modelling the unit root properties of electricity data—A general note on time-domain applications. *Physica A: Statistical Mechanics and its Applications*, *618*, 128685. URL: <https://linkinghub.elsevier.com/retrieve/pii/S0378437123002406>. doi:10.1016/j.physa.2023.128685.
- Smyth, R. (2013). Are fluctuations in energy variables permanent or transitory? A survey of the literature on the integration properties of energy consumption and production. *Applied Energy*, *104*, 371–378. URL: <https://linkinghub.elsevier.com/retrieve/pii/S030626191200801X>. doi:10.1016/j.apenergy.2012.10.069.

- Sobhani, M., Campbell, A., Sangamwar, S., Li, C., & Hong, T. (2019). Combining Weather Stations for Electric Load Forecasting. *Energies*, *12*, 1510. URL: <https://share.goodnotes.com/s/kKVe5tS20xQXvr06Twgmc2>. doi:10.3390/en12081510.
- Svetunkov, I. (2023). *Forecasting and Analytics with the Augmented Dynamic Adaptive Model (ADAM)*. (1st ed.). Boca Raton: Chapman and Hall/CRC. URL: <https://www.taylorfrancis.com/books/9781003452652>. doi:10.1201/9781003452652.
- Verwiebe, P. A., Seim, S., Burges, S., Schulz, L., & Müller-Kirchenbauer, J. (2021). Modeling Energy Demand—A Systematic Literature Review. *Energies*, *14*, 7859. URL: <https://share.goodnotes.com/s/0QajHmV6wgELy0jnbP8Kvs>. doi:10.3390/en14237859.
- Wood, S. N. (2006). *Generalized additive models: an introduction with R*. Texts in statistical science. Boca Raton, FL: Chapman & Hall/CRC. OCLC: ocm64084887.
- Wood, S. N., Goude, Y., & Shaw, S. (2015). Generalized Additive Models for Large Data Sets. *Journal of the Royal Statistical Society Series C: Applied Statistics*, *64*, 139–155. URL: <https://share.goodnotes.com/s/RvmvowVdKEJDUBMfaUby2e>. doi:10.1111/rssc.12068.
- Xie, J., Chen, Y., Davis, K. O., Hong, T., & Laing, T. D. (2018). Relative Humidity for Load Forecasting Models. *IEEE Transactions on Smart Grid*, *9*, 191–198. URL: <https://share.goodnotes.com/s/VSxNWgH4LUeH4YxEXarVEu>. doi:10.1109/tsg.2016.2547964. MAG ID: 2326513046 S2ID: 36d2d0735a40d490e880a67752776666028dd812.
- Zhang, S., Liu, J., & Wang, J. (2023). High-Resolution Load Forecasting on Multiple Time Scales Using Long Short-Term Memory and Support Vector Machine. *Energies*, *16*, 1806. URL: <https://www.mdpi.com/1996-1073/16/4/1806>. doi:10.3390/en16041806.
- Ziel, F. (2018). Modeling public holidays in load forecasting: a German case study. *Modern power systems*, *6*, 191–207. URL: <https://share.goodnotes.com/s/rK6AdeRN4gdJuoJsmrErCA>. doi:10.1007/s40565-018-0385-5. MAG ID: 2792412799 S2ID: 2cd4fed4484bc2ac7e50e890251bdc731d00a11c.
- Ziel, F. (2019). Quantile regression for the qualifying match of GEFCom2017 probabilistic load forecasting. *International Journal of Forecasting*, *35*, 1400–1408. URL: <https://share.goodnotes.com/s/RvmvowVdKEJDUBMfaUby2e>. doi:10.1016/j.ijforecast.2018.07.004.
- Ziel, F. (2022). Smoothed Bernstein Online Aggregation for Short-Term Load Forecasting in IEEE DataPort Competition on Day-Ahead Electricity Demand Forecasting: Post-COVID Paradigm. *IEEE open access journal of power and energy*, (pp. 1–1). URL: <https://share.goodnotes.com/s/kRevXZIZRCVTKMep10sy9F>. doi:10.1109/oajpe.2022.3160933. ARXIV.ID: 2107.06268 MAG ID: 4220944786 S2ID: 9b7f742fc9d1a8d4916225a023d3ce676333a162.
- Ziel, F., & Liu, B. (2016). Lasso estimation for GEFCom2014 probabilistic electric load forecasting. *International Journal of Forecasting*, *32*, 1029–1037. URL: <https://share.goodnotes.com/s/RvmvowVdKEJDUBMfaUby2e>. doi:10.1016/j.ijforecast.2016.01.001.

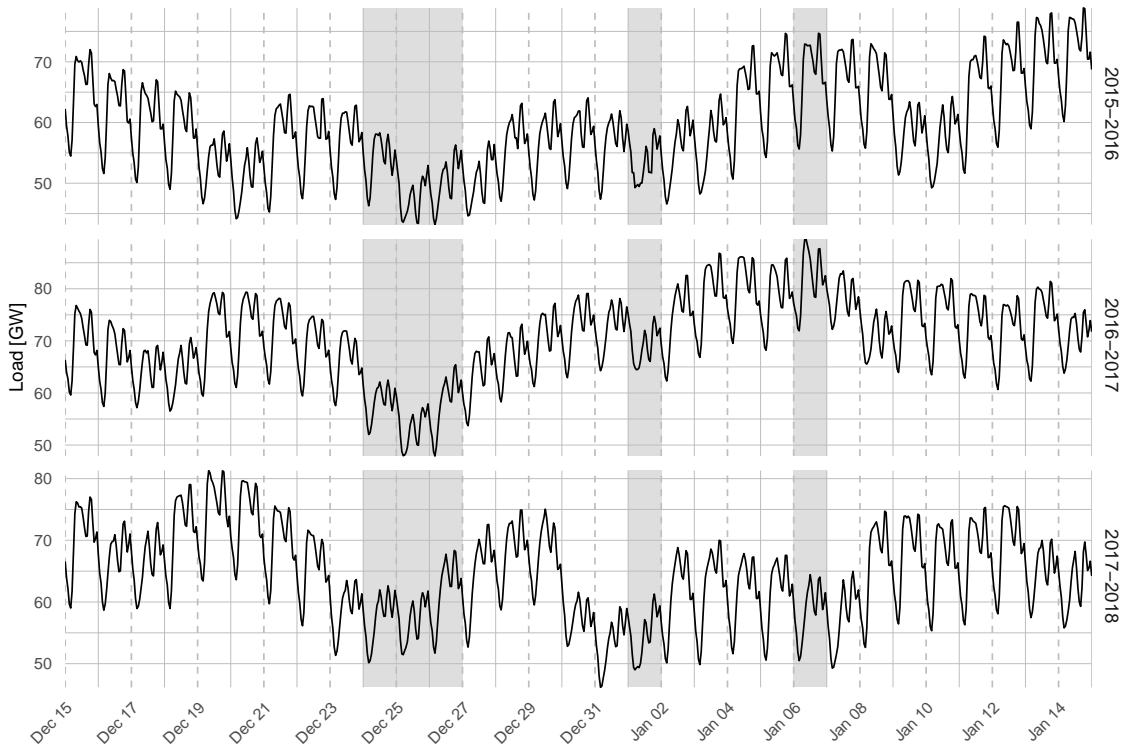
Appendices

A. Appendix: Tabela

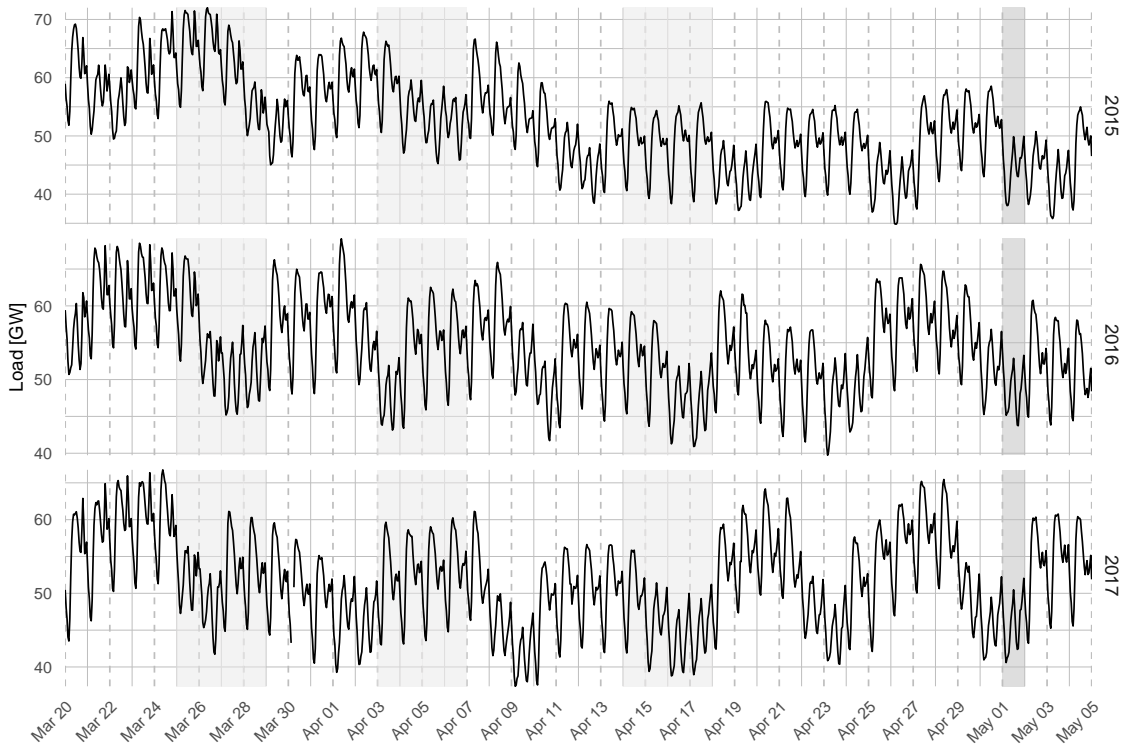
	SRWW	SRWA	STL	VanDet	VanBas	VanRec	ARWD	FNN	GAM	\HLD	\Temp	\States	DA TSO
Austria	1.091	0.627	0.646	1.291	1.217	1.192	0.768	0.495	0.5	0.563	0.519	0.45	0.444
Belgium	1.221	0.731	0.74	1.281	1.213	1.195	0.893	0.647	0.607	0.642	0.629	0.571	–
Bulgaria	1.242	0.439	0.502	0.805	0.694	0.676	0.66	0.379	0.377	0.372	0.357	0.317	0.188
Czech Rep.	1.286	0.583	0.613	1.272	1.137	1.099	0.887	0.456	0.463	0.531	0.486	0.409	0.178
Denmark	0.569	0.336	0.321	0.704	0.669	0.647	0.433	0.312	0.271	0.286	0.275	0.283	0.075
Estonia	0.198	0.091	0.095	0.186	0.153	0.15	0.145	0.073	0.074	0.077	0.078	0.07	0.091
Finland	1.962	1.003	0.899	1.454	0.975	0.961	1.459	0.757	0.727	0.739	0.771	0.712	0.225
France	14.771	6.305	6.257	10.181	7.761	7.621	10.344	5.11	5.039	5.063	5.804	4.778	1.243
Germany	7.157	4.544	4.369	9.519	9.331	9.084	5.171	3.585	3.094	3.702	3.205	3.069	2.645
Greece	1.251	0.754	0.801	1.197	1.176	1.182	0.87	0.62	0.605	0.622	0.65	0.596	0.246
Hungary	0.719	0.439	0.472	0.741	0.73	0.706	0.514	0.349	0.376	0.416	0.393	0.323	0.269
Italy	5.384	3.524	4.14	7.419	7.444	7.406	3.753	2.914	2.975	3.454	3.138	2.532	0.901
Latvia	0.109	0.067	0.064	0.154	0.148	0.145	0.085	0.06	0.046	0.053	0.049	0.052	0.026
Lithuania	0.198	0.116	0.123	0.251	0.241	0.236	0.144	0.097	0.101	0.11	0.102	0.09	0.064
Montenegro	0.087	0.056	0.053	0.084	0.085	0.084	0.066	0.05	0.048	0.048	0.053	0.047	0.037
Netherlands	2.015	1.253	1.627	1.964	1.917	1.88	1.604	1.372	1.2	1.215	1.173	1.282	1.775
Poland	2.454	1.55	1.567	3.208	3.154	3.082	1.693	1.074	1.06	1.389	1.097	0.921	0.677
Portugal	0.769	0.452	0.553	1.006	1.045	1.013	0.534	0.388	0.425	0.448	0.439	0.332	0.226
Romania	0.93	0.615	0.622	1.028	0.987	0.977	0.691	0.505	0.472	0.534	0.515	0.466	0.129
Serbia	0.873	0.467	0.477	0.777	0.651	0.632	0.695	0.504	0.409	0.415	0.435	0.452	0.2
Slovakia	0.459	0.321	0.273	0.496	0.467	0.461	0.348	0.264	0.232	0.25	0.244	0.239	0.118
Slovenia	0.259	0.159	0.156	0.294	0.287	0.28	0.191	0.14	0.125	0.139	0.13	0.13	0.068
Spain	3.601	2.326	2.711	4.404	4.465	4.404	2.643	2.109	2.058	2.307	2.132	1.924	0.427
Sweden	4.102	1.586	1.59	3.073	2.022	1.956	2.941	1.235	1.218	1.246	1.302	1.204	0.532
Sum	52.709	28.343	29.673	52.788	47.968	47.069	37.53	23.494	22.502	24.622	23.978	21.249	10.787

Table 6: Forecasting accuracy in terms of $\overline{\text{RMSE}(\widehat{\mathcal{E}}_h)}$ in GW for $h = 1, \dots, 168 \times 52$ for 24 European countries. The color scheme transitioning from red to yellow and green indicates models ranging from low to high accuracy. The best model for each country is marked by bolt writing. Day-ahead forecasts of the TSO (grey) are considered for countries where less than 1% of forecasts are missing.

B. Appendix: Figures



(a) December 15th in 2015, 2016 and 2017 to January 15th in 2016, 2017 and 2018.



(b) March 1st to May 10th in 2016, 2017 and 2018.

Figure 14: Hourly load in France in the Easter and Christmas holiday time with holidays shaded in grey.

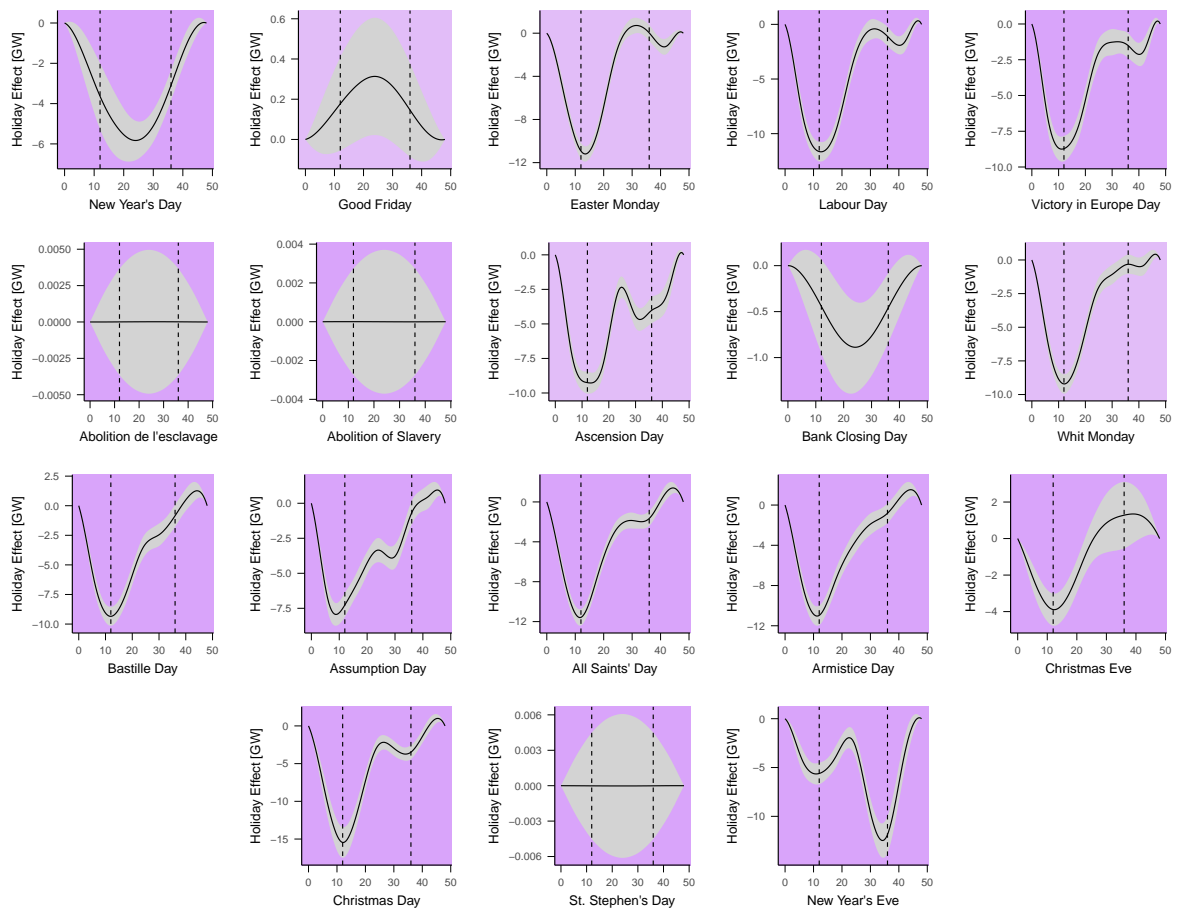


Figure 15: The smooth effects of bridged fixed day (purple) and weekday (light purple) holidays by (7) on load in France with dashed lines indicating the first and last hour of the holiday..

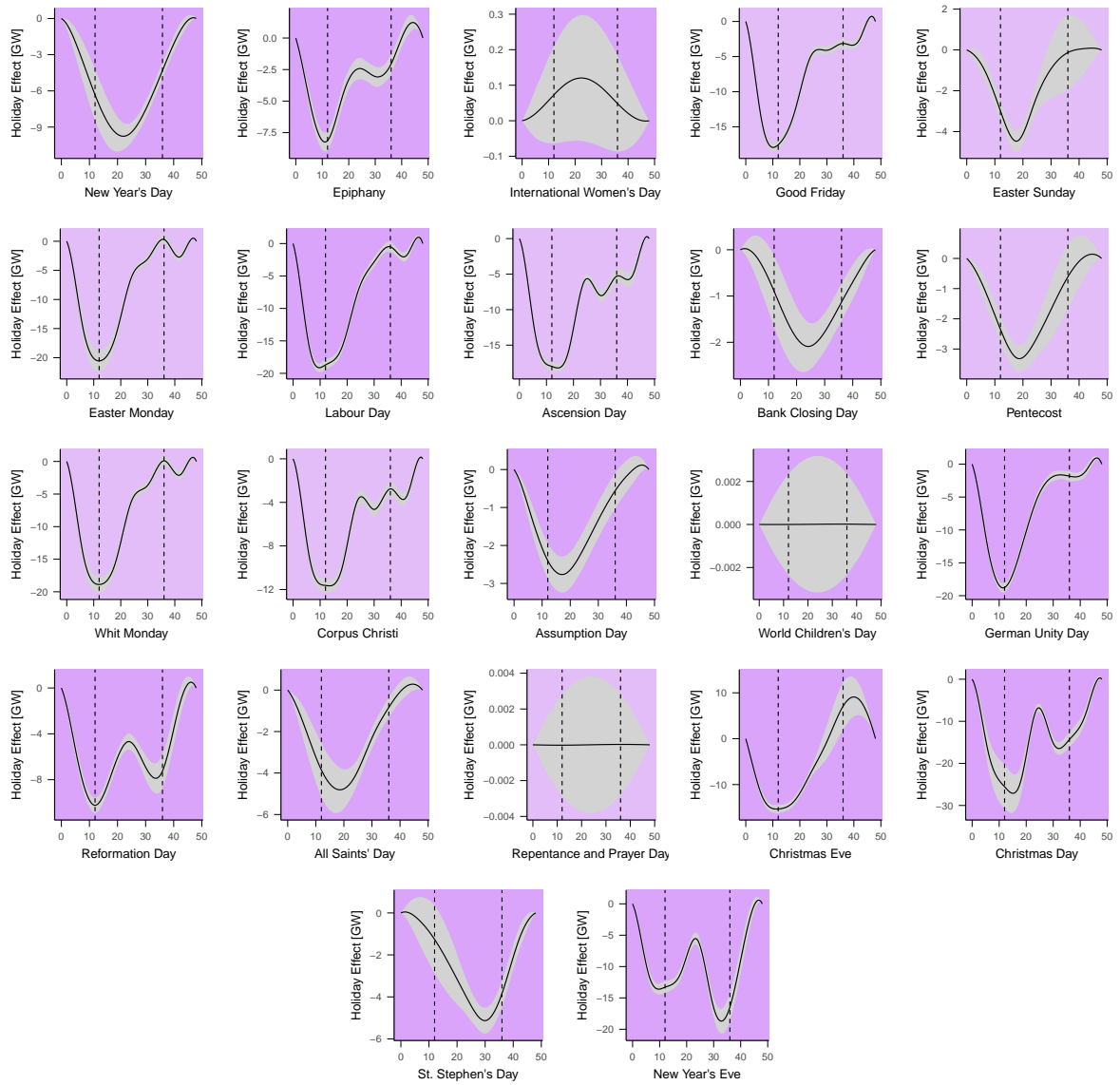


Figure 16: The smooth effects of bridged fixed day (purple) and weekday (light purple) holidays by (7) on load in Germany with dashed lines indicating the first and last hour of the holiday.

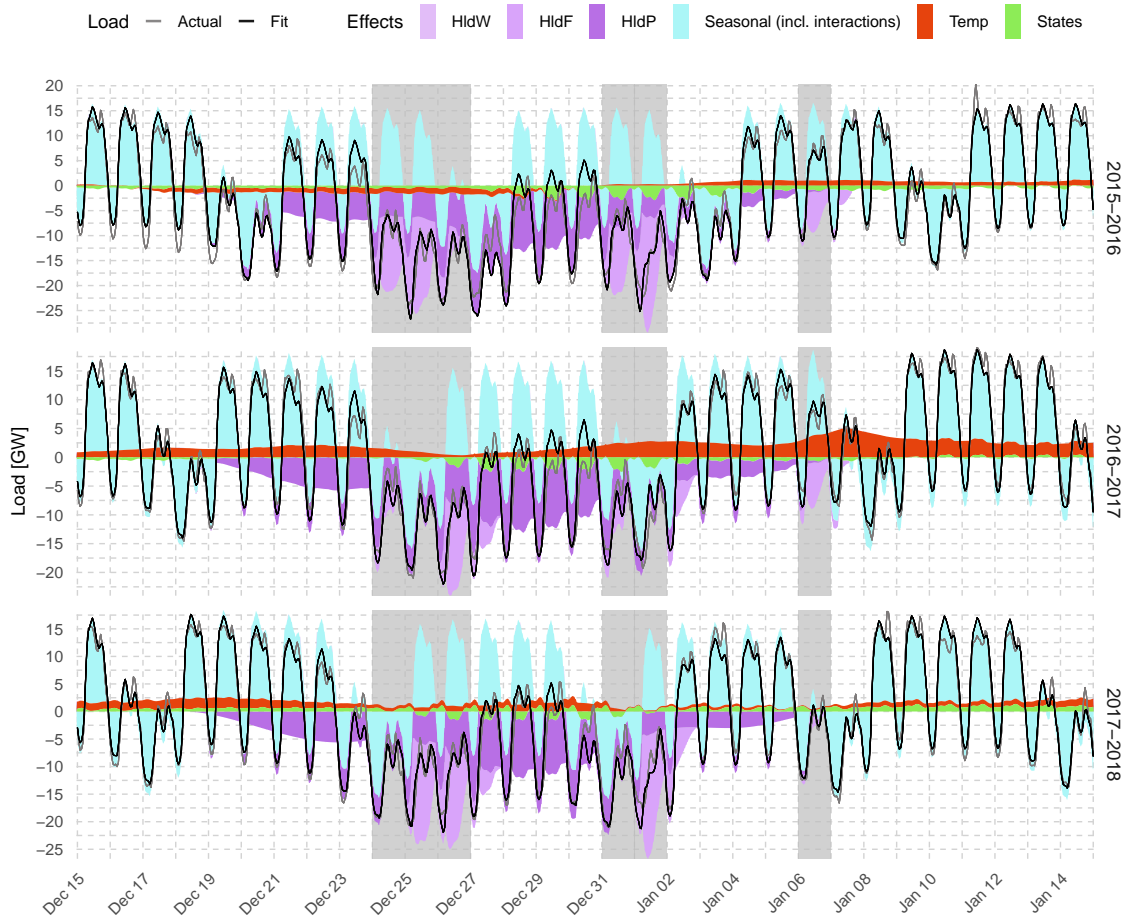


Figure 17: Estimated smooth effects, see (7), on load, fitted and actual load reduced by the estimated intercept in Germany from December 15th 2015, 2016 and 2017 to January 15th 2016, 2017 and 2018, with holidays shaded in grey.

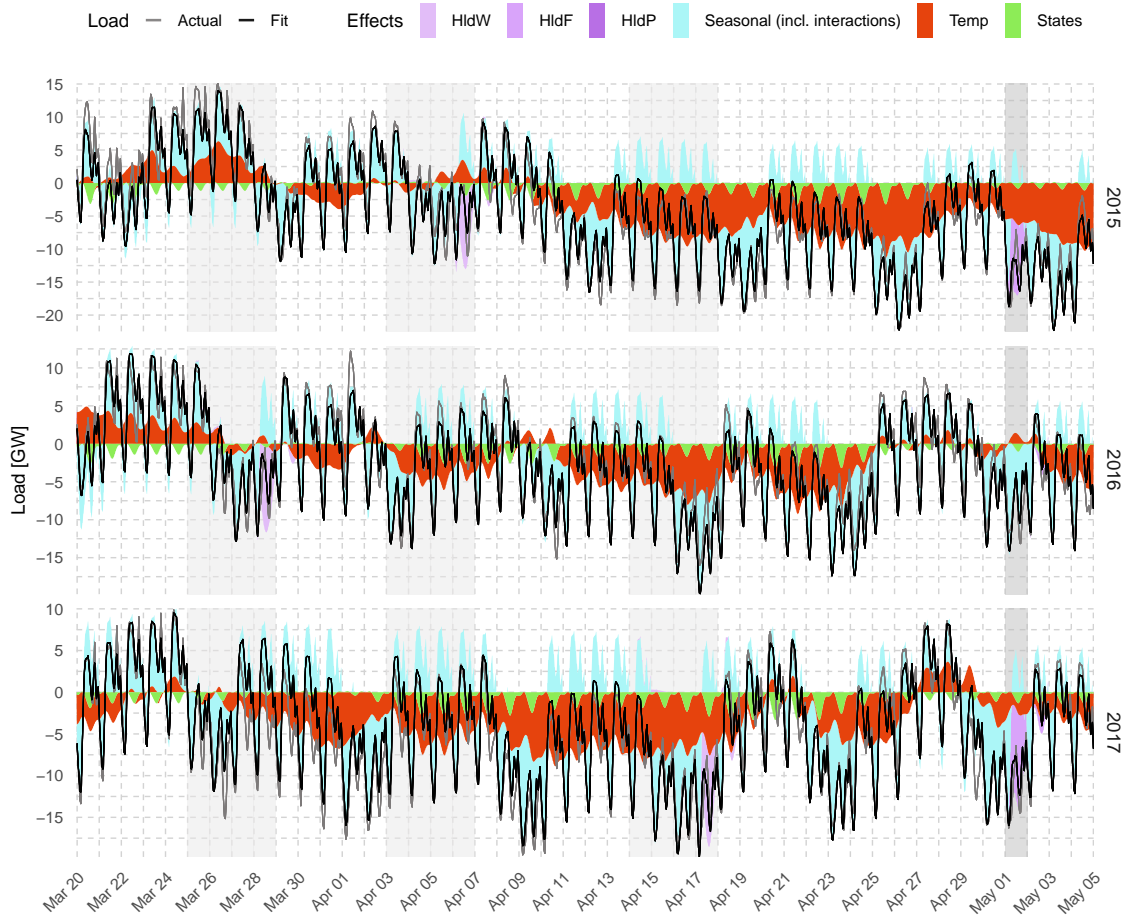


Figure 18: Estimated smooth effects, see (7), on load, fitted and actual load reduced by the estimated intercept in France from March 1st 2016, 2017 and 2018 to May 10th 2016, 2017 and 2018, with weekday holidays shaded in light grey and fixed date holidays shaded in dark grey.